POLITECNICO DI TORINO

Collegio di Ingegneria Chimica e dei Materiali

Corso di Laurea Magistrale

in Ingegneria dei Materiali per l'Industria 4.0

Master thesis

SURFACE MODIFICATION OF BIOFILLERS FOR PRODUCING SUSTAINABLE RUBBER COMPOSITES

Supervisors

Prof. Massimo Messori

Dr. Camilla Noè

Candidate

Saeedeh Saadatyar

Abstract

This research addresses the development of environmentally sustainable natural rubber/styrene butadiene rubber (NR/SBR) composites incorporating a lignocellulosic biofiller derived from winemaking residues (WPL GS+101). To enhance interfacial compatibility between the inherently hydrophilic filler and the hydrophobic rubber matrix, a sequential surface modification strategy was employed: alkali treatment with 2 wt% sodium hydroxides (NaOH), followed by silanization using bis(triethoxysilylpropyl) tetrasulfide (TESPT) at various concentrations of 2%, 5%, and 10 wt%.

Time-resolved alkali treatment was performed over durations of 1, 2, 3, 5, and 24 hours. The effects of surface modification were evaluated through Scanning Electron Microscopy (SEM), Fourier Transform Infrared Spectroscopy (FTIR), and Thermogravimetric Analysis (TGA). SEM images revealed increased surface roughness and fiber exposure. Moreover, FTIR spectra confirmed the removal of hemicellulose and lignin, and TGA results demonstrated enhanced thermal stability in terms of degradation onset and residual mass. According to the data obtained, a duration of 2 hours for alkali treatment was identified as the ideal period to combine with silane treatment.

Following the optimization of alkali treatment duration, silanization was performed to further enhance hydrophobicity and improve filler–matrix compatibilit. In this work, the silane concentration was varied, i.e., 2, 5, and 10 wt.%, based on the WPL GS content. The effect of silane functionalization on the 2%NaOH-treated WPL GS was evaluated using FTIR, SEM coupled with Energy Dispersive X-ray Spectroscopy (EDS), and TGA analysis. The sample treated with 2%TESPT exhibited the most effective surface coverage, achieving a grafting level of 0.76 mmol/g, and was chosen as the biofiller for sustainable rubber composite fabrication.

Various NR/SBR compounds were prepared, differing in the proportions of carbon black (CB) and modified biofiller (2% NaOH-2% TESPT-WPL GS). The CB amounts were varied at 70, 80, 90, 95, and 100 phr relative to total filler content. The mechanical properties of the filled rubber composites, such as tensile strength, elongation at break, hardness, and modulus, were determined. The NR/SBR rubber composite containing 10 phr of modified biofiller achieved a tensile strength comparable to that of the control rubber composite with 100 phr of CB, exhibiting improved stiffness and retained elasticity.

Dynamic Mechanical Thermal Analysis (DMTA) revealed negligible changes in the glass transition temperature (T_g) and the material's damping (tan δ), indicating that the damping properties and molecular mobility were not adversely affected. The Payne effect was consistently lower than control rubber composites, suggesting weaker filler–filler networking and improved dispersion.

Moreover, swelling tests indicated consistent crosslink density and strong filler–matrix compatibility across all loading levels.

In summary, the results demonstrate that NaOH-TESPT-treated WPL can be used as a partial substitute for carbon black—up to 30 phr—without compromising the composite's mechanical, thermal, or dynamic integrity. These findings underscore the viability of modified lignocellulosic fillers as renewable reinforcements in sustainable rubber formulations.

Keywords: Biofiller; Lignocellulose; Surface modification; Sustainable Rubber composites; Green tires.

Contents

Tables

Figures

Table of Abbreviations

Abbreviation	Definition
NR	Natural Rubber
SBR	Styrene-Butadiene Rubber
WPL	Winemaking Process Lignocellulose
TESPT	Bis[3-(triethoxysilyl)propyl] tetrasulfide
NaOH	Sodium Hydroxide
FTIR	Fourier Transform Infrared Spectroscopy
TGA	Thermogravimetric Analysis
DTG	Derivative Thermogravimetry
SEM	Scanning Electron Microscopy
EDX	Energy-Dispersive X-ray Spectroscopy
DMTA	Dynamic Mechanical Thermal Analysis
Tg	Glass Transition Temperature
CB	Carbon Black
Phr	Parts per Hundred Rubber
SA	Stearic Acid
ZnO	Zinc Oxide
TBBS	N-tert-butyl-2-benzothiazyl sulfenamide
ISO	International Organization for Standardization
Q	Swelling Weight Ratio
G'	Storage Modulus
G''	Loss Modulus
ΔG'	Payne Effect
LCA	Life Cycle Assessment
O–H	Hydroxyl Group
Si–O–Si	Siloxane Bond
Si–O–C	Silane–Cellulose Bond
C=O	Carbonyl Group
C–H	Carbon–Hydrogen Bond
C–O	Carbon–Oxygen Bond
Rpm	Revolutions per Minute
°C	Degree Celsius
mm/min	Millimeters per Minute
wt.%	Weight Percent
E'	Storage Modulus (DMTA)
tan δ	Loss Factor (Damping Behavior)
M	Molecular Weight

T_{max}	Maximum decomposition temperature
T_{onset}	Onset decomposition temperature

Introduction

Rubber-based composites have gained significant attention in modern industries due to their versatile applications across various sectors, including automotive, aerospace, sports equipment, adhesives, tires, hoses, gloves, O-rings, conveyor belts, fire-resistant materials, and footwear. The rapid growth of the global economy, particularly in the automotive industry, has resulted in the annual production of millions of tons of tire waste. Improper disposal of this waste poses serious environmental threats. Addressing this issue has become a global priority, with research focusing on innovative methods for recycling and reusing discarded tires. Scientific advancements and changing societal perspectives are driving efforts toward sustainable tire waste management. The demand for sustainable and eco-friendly materials has surged amid rising concerns over environmental pollution, global warming, and the energy crisis. This shift has motivated researchers to explore and develop innovative biocomposite materials that align with ecological objectives while maintaining high performance and functionality [1][2].

Bio composites made from natural fibers and biopolymers offer eco-friendly alternatives to conventional materials. While much research focuses on thermoplastic and resin-based composites, using natural fillers in elastomeric matrices, such as natural rubber (NR), remains less explored. NR is the only bio-based elastomer, valued for its high tensile strength, tear resistance, flexibility, and durability, making it critical to the automotive and transportation industries [3]

Carbon black (CB) is a common reinforcing filler in the rubber industry, enhancing mechanical and thermal properties while influencing vulcanization chemistry. However, its production releases toxic gases and hazardous waste, and it is classified as a Group 2B carcinogen by IARC, posing health and environmental risks. These challenges underscore the need for sustainable, eco-friendly alternatives to replace carbon black in rubber composites [4].

Lignocellulosic fillers are gaining attention as sustainable alternatives in rubber composites due to their renewability, biodegradability, low cost, and favorable mechanical properties. They are composed of cellulose, hemicellulose, and lignin, which have robust and intricate structures. Although this structure provides inherent strength, its hydrophilic nature leads to poor compatibility with the hydrophobic rubber matrix. As a result, rubber composites filled with unmodified lignocellulosic fillers typically exhibit inferior properties compared to those reinforced

with carbon black. For this reason, surface modifications of lignocellulosic fillers are necessary to enhance their compatibility with the rubber matrix [5][6].

Natural fibers can be modified by chemical or physical methods, including alkaline treatment (mercerization), acetylation, silane treatment, benzylation, and the use of coupling agents such as titanates and maleated anhydrides. Among these methods, alkali and silane treatments are the most effective and widely used methods [7][8].

Alkali treatment is a widely used method to enhance the surface properties and chemical reactivity of lignocellulose, making it more suitable for advanced applications in rubber-based composites [9][10]. The primary objective of alkali treatment is to partially remove lignin, hemicellulose, waxes, natural fats, and other impurities that typically inhibit the adhesion of lignocellulose to polymer matrices. By eliminating these elements, the cellulose structure is exposed, revealing more hydroxyl groups on its surface, which significantly increases its chemical reactivity and enhances its ability to form strong bonds with polymer matrices. This process ultimately improves the mechanical and physical properties of the resulting composite [11][12]. In addition, this treatment increases the surface area available for bonding with the matrix, enhances surface roughness, and reduces the surface tension of the filler. Furthermore, the fiber diameter decreases while the fiber aspect ratio increases, improving its reinforcing potential. By partially removing the amorphous regions of hemicellulose and lignin, the alkali treatment also leads to higher crystallinity, contributing to improved structural properties [5]. It also reduces the hydrophilic nature of the material, thereby minimizing moisture absorption — a critical factor in maintaining the durability and stability of the final product under various environmental conditions [7].

The silane treatment process involves several stages, including hydrolysis, condensation, and bond formation, to enhance the properties of natural fibers. During hydrolysis, silanols are formed in the presence of moisture and hydrolyzable alkoxy groups. In the condensation stage, one end of the silanol molecule reacts with the hydroxyl groups of cellulose (forming Si–O–cellulose bonds), while the other end bonds with functional groups in the polymer matrix (forming Si–Matrix bonds). This dual reactivity creates a molecular bridge across the fiber-matrix interface, ensuring improved compatibility and adhesion. Additionally, the hydrocarbon chain provided by the silane prevents fiber swelling within the matrix, further stabilizing the composite's properties. Silane

coupling agents also act as a surface coating, penetrating the micro-pores of natural fibers and forming mechanically interlocked layers that enhance fiber strength [3][10].

Furthermore, silane compounds, with their diverse functional groups, can significantly affect the properties of vulcanizates. Certain compounds, such as vinyltriethoxysilane, participate in rubber cross-linking processes due to the presence of double bonds, while others, like 3,3′-Tetrathiobis(propyl-triethoxysilane), leverage sulfur atoms in their structure for cross-linking. Meanwhile, silanes such as 3-(Aminopropyl) triethoxysilane, 3-(Chloropropyl) triethoxysilane, and octyltriethoxysilane include functional groups that are more compatible with natural rubber, including polar amine or chloride groups and non-polar long carbon chains [3][13].

Several researchers have successfully combined alkali and silane treatments to enhance the properties of natural fiber-reinforced composites, achieving improved interfacial adhesion and mechanical performance [2][8][14]. However, this approach has been relatively underexplored, particularly in applications aimed at developing sustainable tires. In line with these advancements and our goal of developing eco-friendly tire solutions, we employ both treatments to optimize the compatibility of natural fibers with the rubber matrix, ensuring enhanced performance and environmental sustainability.

State of art

2.1. Rubber composites

Rubber-based composites have attracted growing interest due to their versatility in industries such as automotive, aerospace, footwear, biomedical devices, and electronic or thermal applications. They are produced by combining a rubber matrix with reinforcing fillers, resulting in improved mechanical performance, durability, and processability. Rubbers, characterized by unsaturated bonds in their backbone, gain exceptional properties—such as high elasticity, abrasion resistance, and tensile strength—through vulcanization, a crosslinking process that forms a three-dimensional network. However, unfilled rubbers are generally unsuitable for demanding applications and require reinforcement with fillers, along with other additives, to achieve the desired properties. Fillers, typically inorganic or insoluble materials, are crucial in defining composite performance. Their characteristics—size, shape, surface area, aspect ratio, and surface chemistry—govern filler–matrix interactions, influencing strength, resilience, and interfacial adhesion. In nanocomposite systems, however, these intrinsic properties alone are insufficient; the reinforcing effect also depends critically on achieving strong interfacial adhesion between filler and polymer and ensuring uniform dispersion of filler particles within the matrix. [1][5][15].

Fillers are broadly divided into three types based on their reinforcing capabilities: reinforcing, semi-reinforcing, and non-reinforcing fillers. Reinforcing fillers, such as carbon black and silica, possess small particle sizes and improve strength-related properties. Semi-reinforcing fillers offer limited mechanical enhancement, while non-reinforcing fillers, typically with large particle sizes, may even reduce composite strength but are still used to lower production costs [1][5].

2.1.1. Natural rubber

Natural rubber (NR), obtained from the latex of tree is the only commercially available bio-based elastomer and represents a renewable alternative to petroleum-derived rubbers. Chemically, it is cis-1,4-polyisoprene, a polymer known for its exceptional mechanical performance, including high tensile and tear strength, remarkable flexibility, good crack resistance, and low heat build-up during dynamic loading. These properties, combined with its inherent tackiness, make NR highly suitable for demanding engineering applications, particularly in transportation and automotive sectors. As a plant-derived material, NR is inexpensive, widely available, and presents fewer health and environmental hazards compared to synthetic elastomers. While biocomposite research has largely focused on thermoplastics and thermosetting resins, the potential of NR as a natural

polymer matrix in biocomposites reinforced with sustainable fillers is less explored. Leveraging NR's performance and renewable origin offers an opportunity to develop environmentally friendly elastomer-based composites with competitive functional properties [3][16].

2.1.2. Styrene–Butadiene Rubber (SBR)

Styrene–butadiene rubber (SBR) is one of the most widely used synthetic elastomers, valued for its balanced combination of abrasion resistance, aging stability, and process ability. Chemically, SBR is a random copolymer of styrene and butadiene, with its properties being strongly influenced by the styrene-to-butadiene ratio and the microstructure of the butadiene segments. While SBR exhibits good abrasion resistance and low rolling resistance, its tensile strength and elasticity are generally lower than those of natural rubber (NR). Consequently, blends of SBR with NR are often employed to combine the superior tensile and tear strength of NR with the enhanced wear resistance and aging stability of SBR, achieving a synergistic balance suitable for high-performance applications such as tire treads and dynamic rubber goods [17][18].

2.1.3. Conventional Fillers

Carbon black (CB) has long been recognized as the dominant reinforcing filler in rubber manufacturing, particularly in tire production and other high-performance rubber goods. Containing more than 90% elemental carbon, it provides substantial improvements in strength, elasticity, abrasion resistance, and other mechanical properties through strong adhesion at the filler–polymer interface. CB also has the capability to alter the vulcanization chemistry of rubber, exhibiting both chemical and catalytic activity. The overall performance of CB-filled composites depends on several intrinsic factors, including particle size, structural complexity, surface chemistry, and dispersion quality within the rubber matrix. These parameters influence not only static properties such as tensile strength and modulus, but also dynamic behaviors like the Payne effect and Mullins effect, both associated with structural reorganization and energy dissipation during deformation [1][4][5].

Recent advances in filler technology for rubber composites have focused on alternative carbon-based nanofillers, such as graphene, carbon nanotubes (CNTs), and graphite, due to their high surface area, exceptional mechanical strength, and ability to achieve significant reinforcement at low loadings. These materials enable lightweight and high-performance products, although challenges like agglomeration and poor dispersion remain, necessitating surface modification and

hybrid filler approaches. Silica, particularly precipitated silica, is another key reinforcing filler, offering benefits such as reduced rolling resistance, improved fuel efficiency, and enhanced wet grip in "green tires." Its application, however, is limited by poor compatibility with non-polar rubbers, which can be mitigated through silane coupling agents. Emerging hybrid systems, including carbon-coated silica and reduced graphene oxide (rGO), show potential for improved dispersion, lower energy loss, and enhanced abrasion resistance, supporting the development of eco-friendly, high-performance rubber composites [1].

Natural rubber (NR), styrene–butadiene rubber (SBR), and butadiene rubber (BR), which are the main elastomers used in tire manufacturing, have traditionally been reinforced with carbon black (CB) produced from petroleum-derived feedstocks. Its production is highly energy-intensive-consuming approximately 44 GJ of energy and emitting about 3.3 tons of CO_2 for every ton produced [5], and the material itself is non-renewable and non-biodegradable. Furthermore, environmental concerns arise not only from its synthesis but also from handling and disposal processes. The rapid growth of the global automotive industry has also led to the generation of millions of tons of waste tires annually, making their effective disposal a worldwide challenge. In tire manufacturing. These sustainability challenges have intensified the search for renewable, bio-based fillers derived from animal products (e.g., chitosan, chitin), grains (e.g., starch, polysaccharides), plant and wood resources (e.g., lignin, cellulose, natural fibers), agricultural residues, and industrial by-products as alternatives to carbon black (CB) in the rubber industry. These bio-based fillers are biodegradable, lightweight, and cost-effective, with some offering high specific strength and stiffness. Additionally, they possess advantages such as low density, ease of processing, and favorable mechanical properties. Partial substitution of CB with such fillers can reduce rolling resistance by disrupting the CB network (Payne effect) and enhance wet traction due to their hydrophilic nature, though it may slightly reduce wear resistance because bio-fillers are generally softer than CB [1][2][4][5].

2.1.4. Bio-Based Fillers

The growing need for sustainable materials in the rubber industry has encouraged the partial or full replacement of petroleum-derived fillers with natural, plant-based fibers. These lignocellulosic materials are derived from various plant sources, including bast fibres such as jute, flax, ramie, hemp, and kenaf; seed fibres like cotton, coir, and kapok; leaf fibres such as sisal, pineapple, and abaca; as well as fibres from grasses, reeds, wood, and roots [16][19].

The primary building blocks of plant fibres are cellulose, hemicellulose, lignin, pectin, and small quantities of waxes and extractives. Cellulose, a high–molecular weight polysaccharide, is the main load-bearing element that provides mechanical stability, stiffness, and tensile strength. Its structure contains repeating D-anhydroglucose units linked by β-1,4-glycosidic bonds, with hydroxyl groups that form extensive hydrogen bonding networks, directly influencing crystallinity and overall strength. Hemicellulose, present mainly in the primary cell wall, is a branched polymer of mixed sugars that binds to cellulose microfibrils and serves as a flexible matrix. Lignin is a complex aromatic polymer that contributes rigidity, hydrophobicity, and resistance to biological degradation, while pectin enhances structural integrity and flexibility by forming ionic and covalent cross-links. Waxy substances and extractives act as protective layers, influencing fibre colour, moisture uptake, and durability. Although their absolute strength is often lower than that of synthetic fibres, their high specific stiffness, low density, renewability, and reduced environmental footprint make them attractive reinforcements for elastomeric matrices. From a materials engineering perspective, these fibres can be considered natural composites in which cellulose microfibrils are embedded in a hemicellulose–lignin matrix, offering a balanced combination of mechanical reinforcement and sustainability for advanced rubber composite applications [9][10][20][21].

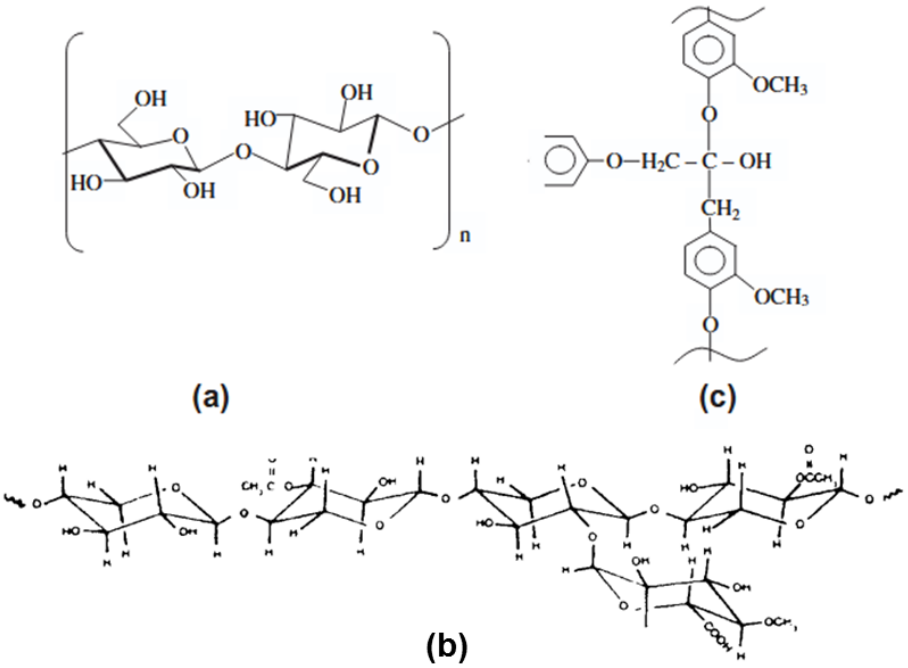

Fig. 1. Representative chemical structures of the primary constituents of lignocellulosic fibres: (a) cellulose, (b) hemicellulose, and (c) lignin [10][12].

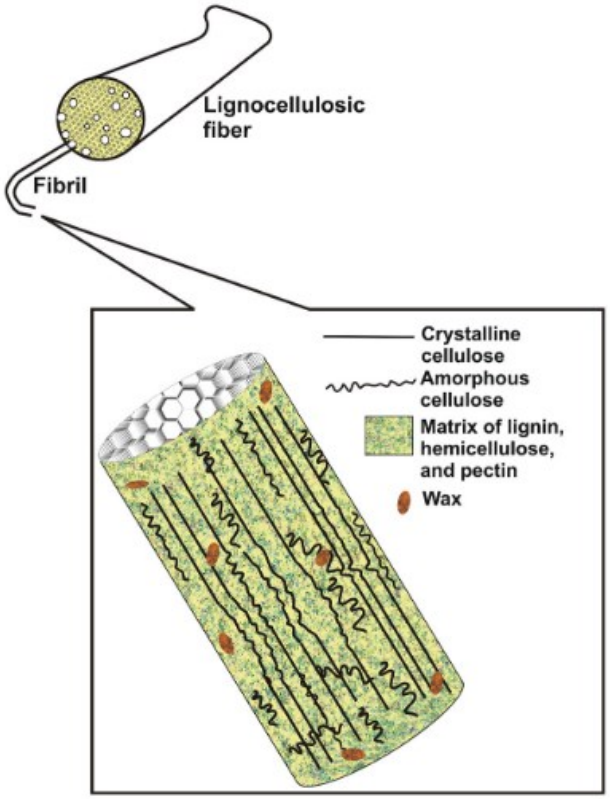

Fig. 2. Schematic representation of the hierarchical structure of lignocellulosic fibres [19].

2.2. Surface Modification Methods

Despite their environmental and performance advantages, bio-based fillers often require surface modification to address the inherent incompatibility between hydrophilic fibres and hydrophobic rubber matrices. The fibre–matrix interface represents a diffusion or reaction zone where the two phases are chemically and/or mechanically combined. Strong interfacial adhesion is essential for achieving desirable mechanical properties in composites; otherwise, weak dispersion of stress across the interface can lead to inferior performance. In the case of natural fibres, the hydrophilic hydroxyl groups present on the fibre surface reduce compatibility with hydrophobic polymer matrices, while pectin and waxy layers further block reactive sites, acting as barriers to mechanical interlocking [10][22][23]. To overcome these limitations, both physical and chemical surface modification methods have been developed to enhance fibre–matrix adhesion.

Physical treatments alter the structural and surface characteristics of fibres without changing their chemical composition. Methods such as stretching, calendaring, thermal treatment, and hybrid yarn production modify surface roughness and improve the mechanical bonding with polymers. Electric discharge methods, including corona and cold plasma treatments, are widely employed for surface activation. These techniques are particularly effective for non-polar polymer substrates such as polyethylene and polypropylene and have been shown to improve filler dispersion and mechanical performance [12][24].

Common chemical treatments include alkaline treatment (mercerization), which removes surface impurities, increases roughness, and activates hydroxyl groups; silane treatment, where silane coupling agents form covalent bonds between fibre hydroxyl groups and the polymer matrix; acetylation, which replaces hydroxyl groups with acetyl groups to reduce moisture absorption; and esterification, in which hydroxyl groups react with acids or anhydrides to improve dispersion. Other approaches such as benzoylation, maleated coupling agents, isocyanate treatments, and polymer grafting have also been investigated to strengthen interfacial bonding. These chemical treatments work by exposing more reactive groups on the fibre surface, enabling stronger coupling with the matrix and improving mechanical performance. Bifunctional coupling agents can remove weak interfacial layers, create durable and flexible interphases, and improve wetting between fibre and polymer. Studies have reported that chemically treated fibres exhibit higher cellulose content, improved thermal stability, increased crystallinity, and enhanced tensile and flexural strength compared to untreated fibres [10][22][23].

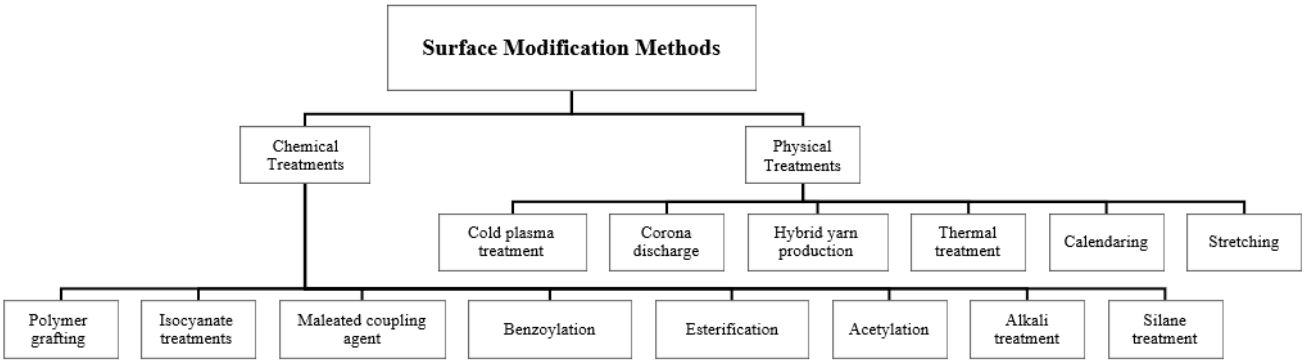

Fig. 3. Classification of surface modification methods for natural fibres.

2.2.1. Alkali treatment

Alkaline treatment, most commonly performed using sodium hydroxide (NaOH), is one of the most effective and widely adopted methods for enhancing the performance of natural fibres (NFs) in polymer composites. This process removes surface impurities such as hemicellulose, waxes, lignin, and fatty substances, thereby improving fibre–matrix adhesion, moisture resistance, and thermal stability [23][25][26].

Physicochemical and structural changes such as the loss of hydrogen bonds and an increase in the amorphous fraction at the expense of crystalline regions, lead to the generation of alkali–cellulose intermediates (soda–cellulose), which can subsequently transform into regenerated cellulose (cellulose II) upon removal of unreacted NaOH and drying. These crystalline transitions alter the mechanical characteristics of the fibres and increase the number of reactive hydroxyl sites available for bonding with the matrix. In addition, hydrogen peroxide can be used under alkaline conditions to further remove hemicellulose, lignin, and other surface contaminants [11].

The efficiency of alkali treatment depends on several parameters, including NaOH concentration, temperature, immersion time, and fibre-to-solution ratio. Higher concentrations and elevated temperatures tend to remove which removes amorphous constituents (hemicellulose and lignin), thereby exposing the crystalline cellulose microfibrils and promoting stronger hydrogen bonding between them. This removal of non-cellulosic components, combined with the subsequent close-packing of the remaining microfibrils, results in a reduction in fibre diameter, improved surface roughness, and enhanced tensile strength, all of which are beneficial for their role as reinforcement in polymer composites [25].

Despite its advantages, alkali treatment can also cause fibre degradation if not carefully controlled, and it generates chemical waste that requires proper disposal to maintain environmental sustainability [23]. Therefore, optimisation of process parameters is essential to balance performance improvements with fibre integrity and environmental considerations.

2.2.2. Silane treatment

Silane coupling agents are highly effective in modifying the surface of natural fibres to enhance their compatibility with polymer matrices. In most practical approaches, silane treatment is combined with an alkali pre-treatment. Without alkali activation step, silane modification remains limited to superficial sites, as the highly hydrogen-bonded structure of cellulose restricts molecular penetration [6].

Silane coupling agents are widely recognized as highly effective modifiers for improving the compatibility of natural fibres with polymer matrices. Their unique functionality lies in the simultaneous presence of hydrolysable alkoxy groups and organofunctional groups. In the presence of moisture, alkoxy groups hydrolyze into silanols, which react with hydroxyl groups on the fibre surface, while the organofunctional ends interact with the polymer chains. Through these reactions, stable covalent networks are formed at the fibre–matrix interface, which transform the fibre surface from hydrophilic and moisture-sensitive into hydrophobic and chemically active [11][19][23].

While silane functionalisation provides improved dispersion, enhanced wettability, and higher mechanical interlocking within composites, its industrial application must also consider processing cost, compatibility with specific polymer systems, and the environmental aspects of silane waste management. With appropriate handling, silane agents remain a highly versatile tool for sustainable natural fibre modification in polymer composites [23].

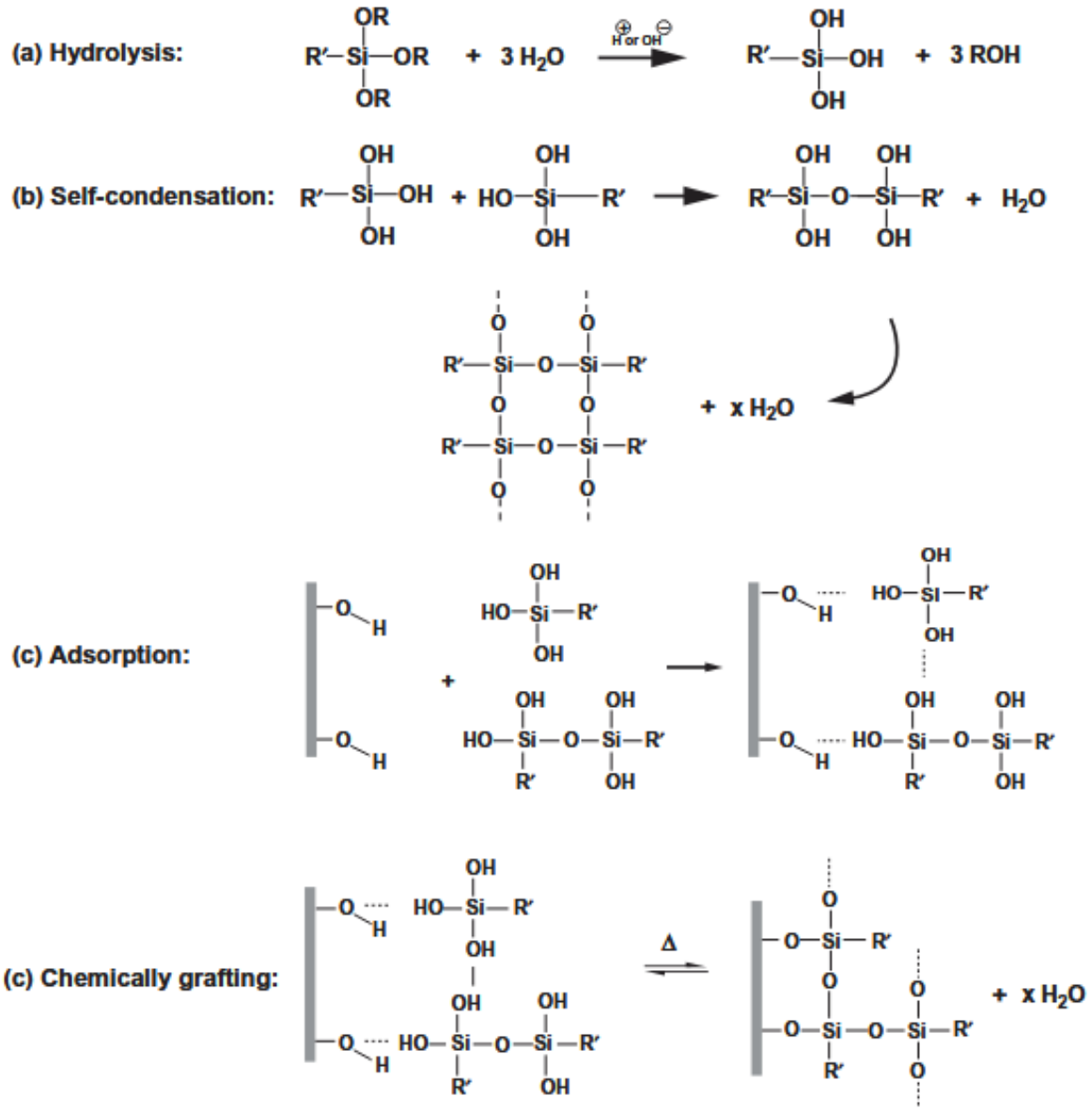

Fig. 4. Interaction of silane with natural fibres through: (a) hydrolysis, (b) self-condensation, (c) adsorption, and (d) chemical grafting, leading to stable siloxane linkages and improved fibre–matrix adhesion[6].

2.3. Impact on Composite Properties

2.3.1. Mechanical performance

Saha et al. [27] examined the tensile behavior of lignocellulosic jute fibers subjected to alkali treatment under both ambient and elevated temperatures, as well as alkali–steam treatment. Their study aimed to determine how these treatment conditions influenced uniaxial tensile strength. The findings indicated that alkali–steam treatment yielded the most pronounced improvement in tensile strength compared to untreated fibers and those treated at ambient temperature. This enhancement

was primarily linked to the effective removal of hemicellulose and surface contaminants, which promoted fibrillation and improved stress transfer efficiency within the fiber structure.

In line with this observation, Widodo et al. [28] evaluated the mechanical performance of Sansevieria trifasciata fibers (STF) before and after NaOH treatment through single-fiber tensile testing. The alkali-treated fibers demonstrated marked increases in both tensile strength and modulus. These gains were associated with the removal of amorphous non-cellulosic materials, resulting in stronger inter-fibrillar bonding, improved load-bearing capacity, and reduced fiber slippage during tensile deformation.

Building on the role of surface modification in improving reinforcement, Kaewsakul et al. [13] conducted a comparative study on the effectiveness of different silane coupling agents in rubber composites. Five silanes were investigated: bis-(triethoxysilylpropyl) tetrasulfide (TESPT), bis-(triethoxysilylpropyl) disulfide (TESPD), octyltriethoxysilane, vinyltrimethoxysilane, and bis-(trimethylsilylmethyl) tetrasulfide (TMSMT), with TESPT selected as the reference. They reported that sulfur-containing silanes (TESPT, TESPD) markedly improved the tensile strength and modulus of rubber composites due to their dual ability to bond with filler hydroxyl groups and to participate in vulcanization. In contrast, non-sulfur silanes (octyltriethoxysilane, vinyltrimethoxysilane) showed limited reinforcement because of weaker filler–matrix adhesion. Furthermore, Payne effect measurements revealed that sulfur-functional silanes, such as TESPT and TESPD, significantly reduced filler–filler interactions and enhanced silica dispersion within the rubber.

Similarly, Miedzianowska et al. [3] reported that silane-modified horsetail fillers (APTES, CPTES, OTES, VTES, TESPT) significantly improved the mechanical behavior of NR composites compared to untreated fillers. The hardness and tensile strength (TS) increased with filler loading up to 20 phr, with APTES and TESPT showing the most pronounced reinforcement due to their functional groups (amino and sulfur) enhancing vulcanization and filler–rubber bonding. However, elongation at break (Eb) decreased for APTES, VTES, and TESPT systems, reflecting higher crosslink density. Dynamic mechanical tests further showed a reduced Payne effect ($\Delta G'$) for silane-treated composites, indicating suppressed filler–filler networking and improved dispersion. This was attributed to the reduction of hydroxyl groups on horsetail fibers after silanization, which limited hydrogen bonding and aggregation, consistent with FTIR evidence.

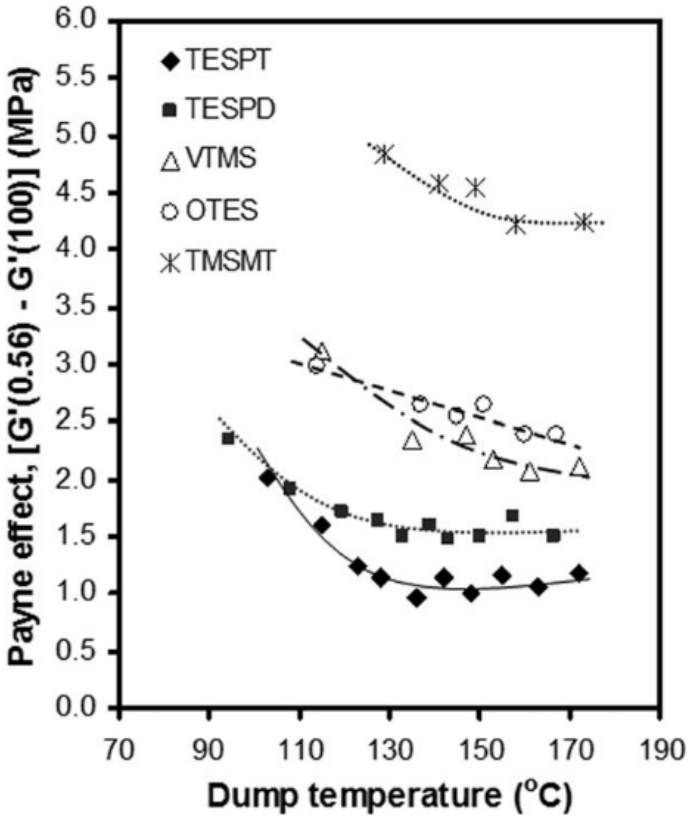

Fig. 5. Payne effect of silica-filled NR compounds modified with different silane coupling agents (TESPT, TESPD, VTMS, OTES, and TMSMT) as a function of dump temperature [13].

Extending these findings to jute fiber–reinforced NR systems, Roy et al. [14] investigated the effect of different surface treatments, including alkali, alkali/stearic acid, and alkali/silane modifications. They reported that the addition of untreated fibers slightly improved stiffness but reduced tensile strength because of weak interfacial bonding. When the fibers were chemically modified, especially through combined alkali and silane treatment, the composites exhibited clear improvements in modulus, hardness, and tensile strength. This enhancement was attributed to better dispersion of the fibers, increased crosslink density, and stronger interfacial adhesion, which together facilitated more efficient stress transfer from the rubber matrix to the fibers. However, all fiber-filled composites showed lower elongation at break compared to neat rubber, reflecting increased stiffness and reduced flexibility.

Table 1. Mechanical properties of natural rubber (NR) composites reinforced with untreated and surface-treated jute fibers [14].

Formulation	M_{100} (MPa)	Hardness (Shore A)	Tensile Strength (MPa)	Elongation at Break (%)	Crosslink Density $\times 10^5$ (mol cm^{-3})
Unfilled NR	0.83 ± 0.04	47 ± 2	12.07 ± 0.58	835 ± 15	7.21
NR/JF_{un}	1.20 ± 0.09	55 ± 2	10.52 ± 0.69	765 ± 15	8.54
NR/A-JF	1.49 ± 0.07	58 ± 1	14.21 ± 0.89	750 ± 20	8.76
NR/A-St-JF	1.63 ± 0.12	59 ± 1	15.91 ± 0.44	750 ± 20	9.01
NR/A-Si-JF	1.77 ± 0.11	62 ± 2	17.04 ± 0.52	770 ± 20	10.88

2.3.2. Thermal stability

Widodo et al. [28] assessed the thermal performance of alkali-treated Sansevieria trifasciata fibers using thermogravimetric analysis (TGA). Their findings showed a moderate upward shift in the onset degradation temperature compared to untreated fibers, indicating enhanced thermal resistance. This improvement was linked to the removal of hemicellulose and lignin, which left a thermally more stable cellulose-rich structure.

In a related study, Raia et al. [29] examined the thermal stability of Pinus fibers subjected to a range of NaOH concentrations (1–4 wt.% and above) and varying immersion periods. TGA/DTG curves demonstrated that intermediate alkali levels and controlled treatment times promoted the selective removal of hemicellulose and lignin, thereby delaying thermal decomposition.

Conversely, overly strong alkali solutions or extended treatment durations partially degraded cellulose, resulting in a reduction in thermal stability.

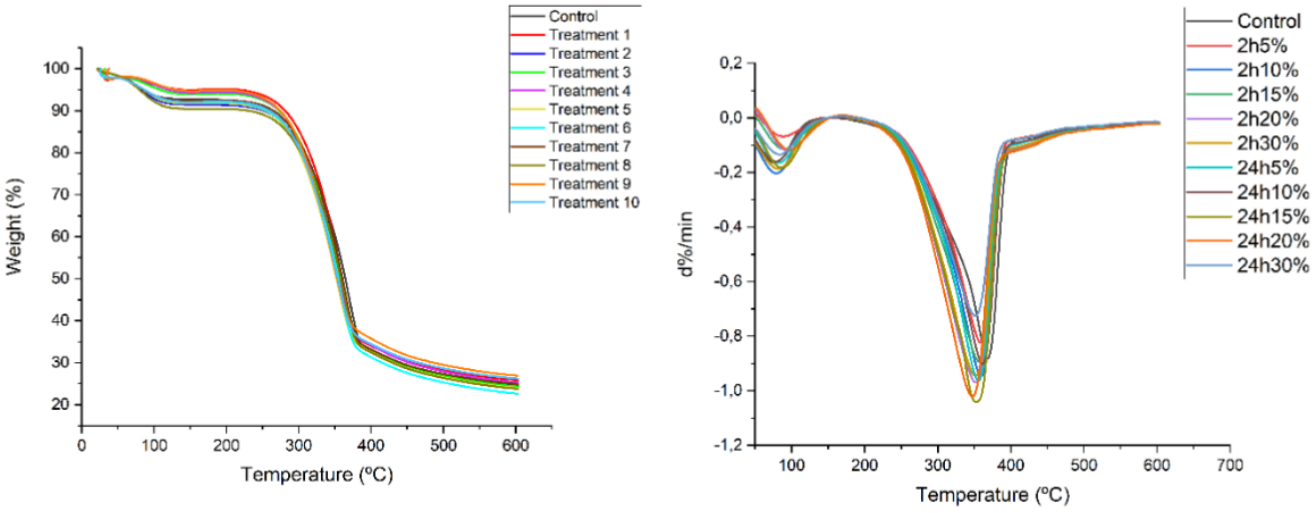

Fig. 6. TGA and DTG curves of untreated and alkali-treated Pinus fibers at different NaOH concentrations (5–30%) and times (2 h, 24 h), showing the effect of treatment on thermal stability [29].

Expanding on the influence of chemical modification, Miedzianowska et al. [3] investigated the thermal stability of horsetail fibers treated with different silanes (APTES, CPTES, OTES, VTES, TESPT) using TGA/DTG. Silanized samples showed lower initial moisture loss (3–4% vs. 8% for untreated), higher T50 values, and greater residues at 800 °C, indicating improved thermal stability. The modification reduced hydrophilicity and enhanced filler compatibility with rubber matrices. Similarly, Thermogravimetric analysis (TGA) performed by Gieparda et al. [22] revealed differences in the thermal behavior of fibers subjected to different treatments. Alkali treatment slightly increased thermal stability by eliminating amorphous components. Further silane functionalization enhanced this effect: GPS-treated fibers showed the highest onset of decomposition temperature and the greatest resistance to thermal degradation, while APS-treated fibers also exhibited improved stability compared to untreated samples.

At the composite level, Roy et al. [14] studied the thermal stability of NR composites with untreated and surface-treated jute fibers. No clear change was observed in the initial degradation (T10%, T20%). However, NR with alkali/silane-treated fibers showed slightly higher T50% and

T80%, indicating improved stability due to stronger rubber–fiber interactions that limited chain mobility and delayed degradation.

2.3.3. Chemical Structure

Raia et al. [29], used the Fourier Transform Infrared Spectroscopy (FTIR) spectroscophy to assess chemical modifications in fibers subjected to alkali treatment under varying conditions. The spectra showed a marked reduction or complete disappearance of characteristic absorption peaks associated with hemicellulose and lignin, confirming their partial removal. The treatment also led to the exposure of cellulose hydroxyl groups, thereby improving the potential for chemical bonding with hydrophobic polymer matrices. Similarly, FTIR analysis by Widodo et al. [28], revealed diminished hemicellulose- and lignin-related peaks in alkali-treated fibers, accompanied by increased intensity of cellulose-specific absorption bands.

Beyond alkali modification, silane treatments produced more pronounced chemical changes. Miedzianowska et al. [3] studied horsetail biofiller modified with different silane coupling agents, namely VTES, TESPT, APTES, CPTES, and OTES. Using FTIR spectroscopy, they confirmed that silanization altered the chemical structure of the fibers. The treatment reduced hydroxyl-related absorbance bands, indicating the reaction of silane groups with cellulose. At the same time, new absorption bands associated with Si–O–C and Si–O–Si bonds appeared, confirming the formation of polysiloxane structures on the fiber surface.

According to Gieparda et al. [22], Alkali-treated fibers showed reduced intensities of peaks associated with hemicellulose and lignin, confirming their partial removal. In addition, silane treatments introduced new absorption bands attributed to Si–O–C and Si–O–Si linkages, indicating successful grafting of silane molecules onto the cellulose surface. GPS-treated fibers demonstrated stronger characteristic peaks compared to APS-treated ones, suggesting a more effective surface functionalization. Among the silane coupling agents, γ-glycidoxypropyltrimethoxysilane (GPS), which contains an epoxy functional group, demonstrated stronger characteristic peaks compared to γ-aminopropyltriethoxysilane (APS), which carries an amino group. This suggests that GPS was more effective in surface functionalization, as its epoxy group provided stronger bonding and reduced hydrophilicity, while APS mainly enhanced chemical reactivity through its amino functionality.

2.3.4. Morphology and dispersion

To evaluate surface morphology, Raia et al. [29] **investigated untreated and alkali-treated fibers using Scanning Electron Microscopy (SEM). Varying NaOH concentrations and treatment durations resulted in a progressive removal of surface impurities such as waxes and pectins, accompanied by increased surface roughness and fibrillation. These changes are expected to enhance fiber wettability and facilitate stronger mechanical interlocking in composite matrices. Similarly, Saha et al.** [27] **reported that treated jute fibers exhibited cleaner surfaces with pronounced fibrillation compared to untreated fibers, which retained waxy layers and other impurities. In their study, alkali–steam treatment produced a more uniform and rougher surface, conditions that favor improved interfacial adhesion in composite applications.**

Gieparda et al. [22] investigated the morphology of flax fibers before and after alkali and silane treatments using SEM. Untreated fibers displayed a relatively smooth surface covered with waxes and impurities. After alkali treatment, the fibers exhibited a rougher and cleaner surface, indicating the removal of hemicellulose and surface contaminants. Subsequent silane treatments with 3-aminopropyltriethoxysilane (APS) and 3-glycidoxypropyltrimethoxysilane (GPS) further modified the fiber surface, producing more homogeneous coatings and suggesting improved interfacial compatibility with polymer matrices.

Experimental

3.1.Materials

The primary material used in this study was WPL GS+ 101, a natural biofiller derived from winemaking by-products, primarily sourced from the Emilia-Romagna region in Italy. WPL GS+ 101 has a moisture content of less than 3wt% and demonstrates excellent thermal stability, with a T15 at 271°C. Its fine particle size and density (1.60 g/cm^3) make it suitable for reinforcing polymer composites, improving thermo-mechanical properties.

In this study, sodium hydroxide was used as the primary reagent for alkali treatment due to its ability to effectively remove lignin, hemicellulose, waxes, and other impurities from natural lignocellulosic materials.

Acetic acid, with an analytical grade purity of at least 99.5%, was used to alkali-treat WPL GS. This step was crucial in stabilizing the modified lignocellulosic structure and preventing potential degradation during further processing.

Other ingredients were provided by Michelin company including NR, SBR, CB N326 (with average pore size ~27 nm and BET surface area ~77 m^2/g), oil, zinc oxide (ZnO) as an activator, stearic acid (SA) as a curing/release agent, sulfur as a vulcanizing agent, and N-tert-butyl-2-benzothiazyl sulfenamide (TBBS) as an accelerator. All components were used as received without further purification.

The main chemicals and materials used in the surface treatment and composite formulation processes are illustrated in Figures 7 and 8, respectively.

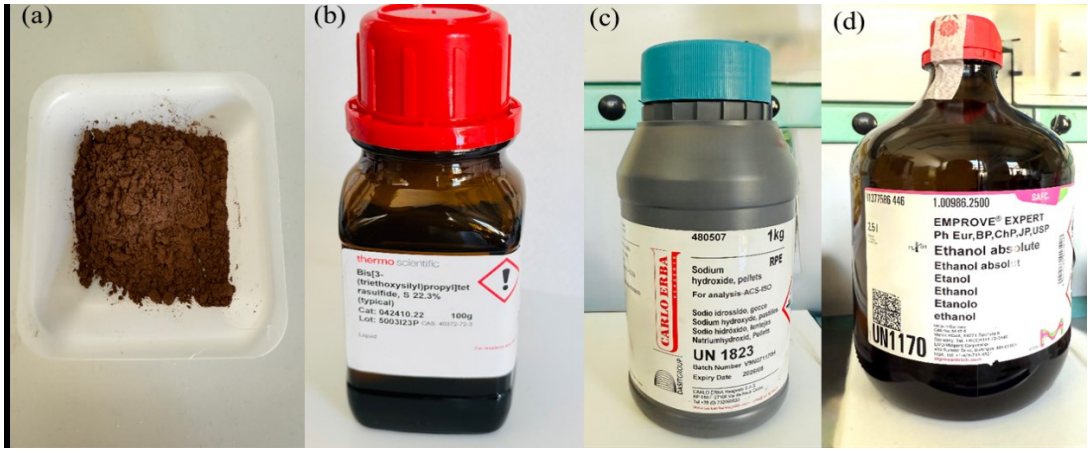

Fig. 7. Materials used for WPL GS surface treatment : (a) Untreated WPL powder, (b) TESPT silane, (c) NaOH pellets, (d) Absolute ethanol.

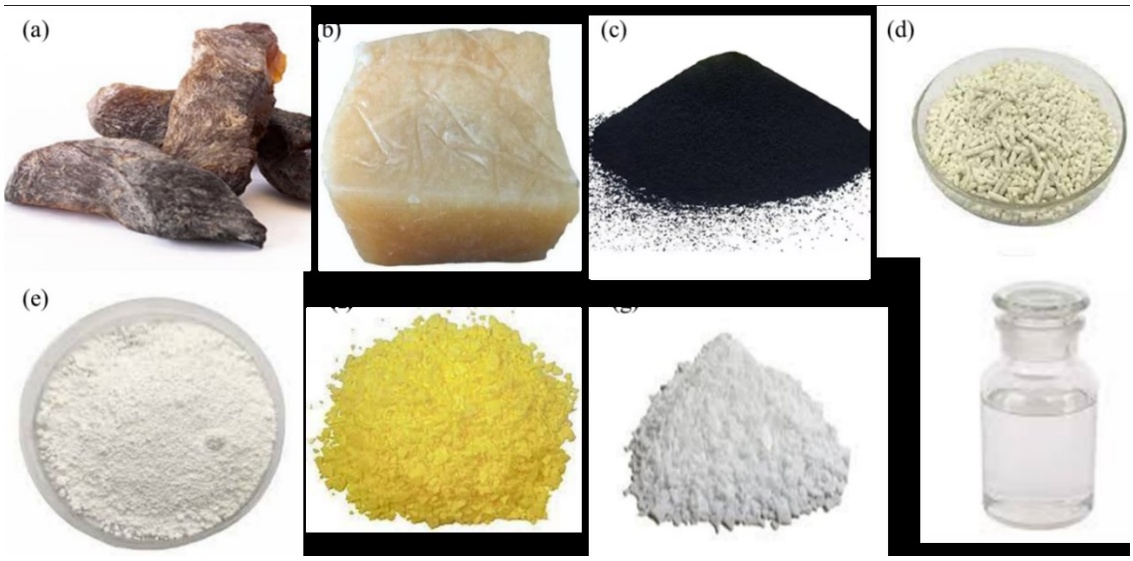

Fig. 8. Raw materials used in NR/SBR composite preparation: (a) Natural rubber (NR), (b) Styrene-butadiene rubber (SBR), (c) Carbon black, (d) TBBS accelerator,
(e) Zinc oxide, (f) Sulfur, (g) Stearic acid, (h) Processing oil.

3.2. Method

3.2.1. Fiber surface treatment

For the alkali treatment, as-received untreated WPL powders were immersed in 2wt% NaOH solutions by maintaining a fiber weight to alkali volume ratio of 1:50 at ambient temperature (25 ± 2 °C) for various times of 1h, 2h, 3h, 5h, and 24h. Then, the alkali-treated WPL was neutralized with diluted acetic acid. The powders were collected by centrifugation and washed with distilled water several times until the fiber's surface was entirely free from the unreacted alkali. The obtained samples were dried in the oven at 70 °C until a constant weight was obtained. The alkali-treated samples were denoted as 2%NaOH-WPL-1h, 2%NaOH-WPL-2h, 2%NaOH-WPL-3h, 2%NaOH-WPL-5h, and 2%NaOH-WPL-24h, corresponding to the process times. Among these, the 2-hour treatment (2%NaOH-WPL-2h) was found to be optimal based on the characterization results.

In the combined alkali-silane treatment, an ethanol-water mixture (60:40) was first prepared. Then, acetic acid was added to adjust the pH of the solution to about 4.5. After that, TESPT was added to the solution at various concentrations of 2, 5, and 10 wt.%, considering the content of NaOH-treated WPL, and stirred at room temperature (RT) for 2 hours to achieve a uniform dispersion. Next, 4 g of alkali-treated WPL (2%NaOH-WPL-2h) was added into 100 mL of the prepared silane solution, and stirring continued for an additional 3 hours to complete the

silanization process. Silylated samples were collected by centrifugation, washed multiple times with distilled water to eliminate unreacted silane, and dried at 70 °C for 24 hours. The treated samples were named 2%NaOH-WPL-2TESPT, 2%NaOH-WPL-5TESPT, and 2%NaOH-WPL-10TESPT based on the silane concentration. Based on the preliminary characterization results, the 2%NaOH-WPL-2TESPT formulation was selected as the designated biofiller for the subsequent fabrication of rubber composites.

3.2.2. Preparation and curing of rubber composites

Various NR/SBR compounds were formulated with different proportions of carbon black (CB) and 2%NaOH-WPL-2TESPT, as detailed in Table 2. The mixing process was conducted using a Brabender laboratory mixer (MT 1902140.1289), equipped with a 45 cm^3 mixing chamber, at 110 °C and a rotational speed of 90 rpm (Figure 9).

The process began with the charging of NR into the mixer, followed by blending for 5 minutes. Subsequently, SBR was introduced and mixed until a nearly homogeneous blend was achieved. Then, Stearic acid and zinc oxide were added to ensure uniform dispersion. In the next step, half of the CB and half of the oil were incorporated into the mixture. Once proper dispersion was achieved, the remaining CB and oil were added. The CB content varied between 70 and 100 phr, based on the total filler content.

Afterward, 2%NaOH-WPL-2TESPT, in amounts ranging from 5 to 30 phr, was gradually introduced into the mixer and blended for 2 minutes. In the final stage, sulfur and TBBS were added and mixed until a uniform rubber compound was obtained. The resulting rubber composite was molded into 1 mm-thick sheets using a Gibitre hot plate press, operated at 140 °C for 12 minutes. The treated WPL-reinforced rubber composites were designated based on their biofiller content as follows: 100CB (Control), 2%NaOH-5WPL-2TESPT, 2%NaOH-10WPL-2TESPT, 2%NaOH-20WPL-2TESPT, and 2%NaOH-30WPL-2TESPT.

Table 2. Formulation data of the prepared rubber composites at different CB/treated-WPL ratios (Parts per hundred rubber).

Ingredients	100CB (Control)	2%NaOH-5WPL-2TESPT	2%NaOH-10WPL-2TESPT	2%NaOH-20WPL-2TESPT	2%NaOH-30WPL-2TESPT
NR	100	100	100	100	100
SBR	100	100	100	100	100
SA	2	2	2	2	2
ZnO	5	5	5	5	5
CB	100	95	90	80	70
Oil	40	40	40	40	40
2%NaOH-WPL-2TESPT	0	5	10	20	30
Sulfur	4	4	4	4	4
TBBS	6	6	6	6	6

Fig. 9. Brabender Plastograph internal mixer used for compounding NR/SBR rubber composites.

The comprehensive experimental procedures for the alkali treatment of the WPL GS biofiller, its subsequent TESPT silane functionalization, and the preparation of biofiller-reinforced NR/SBR rubber composites are summarized in Figure 10.

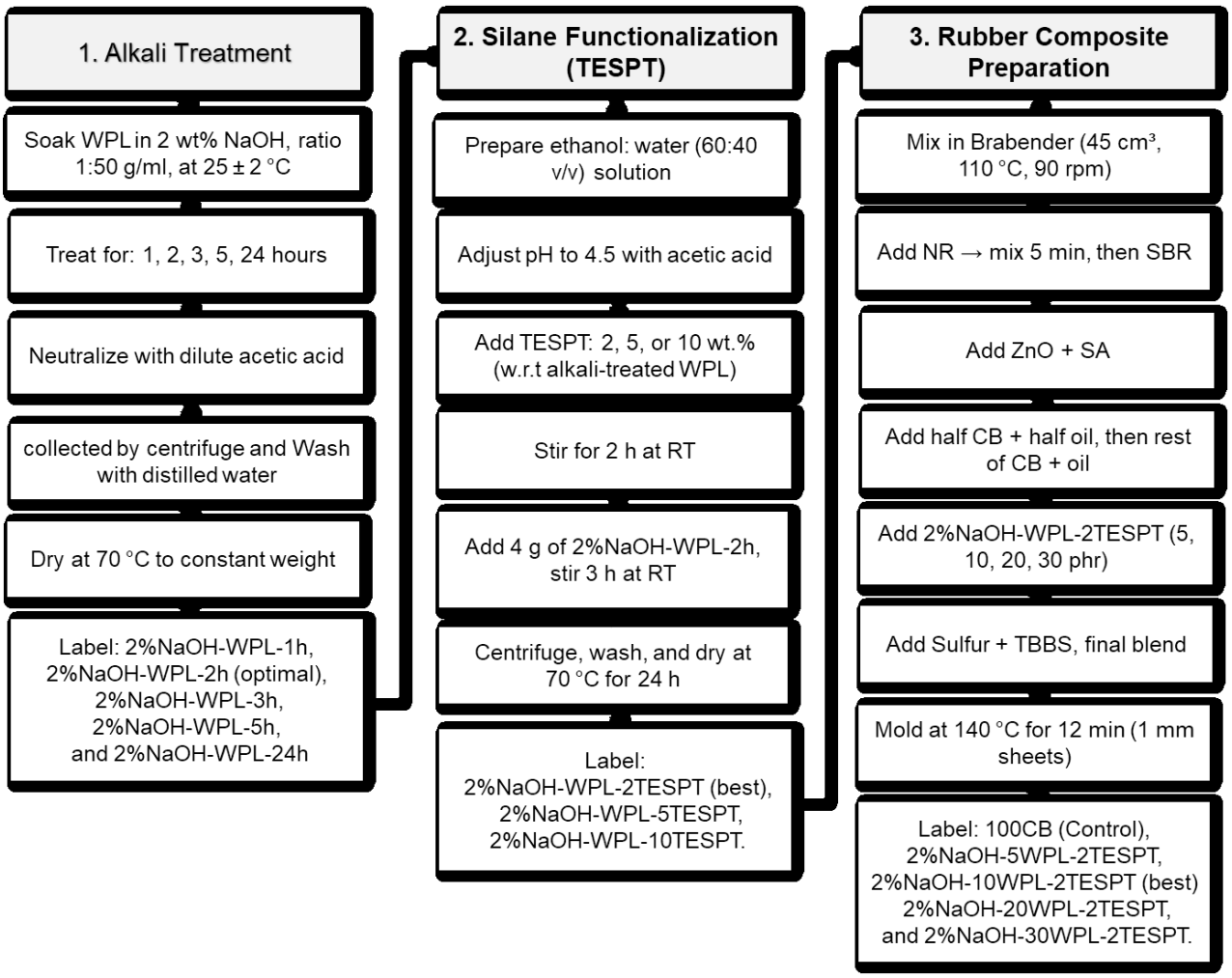

Fig. 10. Schematic workflow of WPL surface modification and NR/SBR composite preparation, including alkali treatment, TESPT functionalization, and rubber compounding with molding.

3.3.Characterization

Advanced analytical methods were employed to assess the chemical, structural, and thermal properties of both treated and untreated WPL and reinforced-rubber composites.

3.3.1. Scanning Electron Microscope

Scanning Electron Microscopy (SEM) is a high-resolution imaging technique that uses a focused beam of high-energy electrons to scan the surface of a specimen. As the electrons interact with the atoms of the sample, several signals are generated, including secondary electrons, which are used to form detailed images of surface morphology. The technique provides topographical, compositional, and, in some cases, crystallographic information at the microscale.

Energy-Dispersive X-ray Spectroscopy (EDS), often integrated with SEM, is used to analyze the elemental composition of a material. When the electron beam strikes the sample, it can eject

inner-shell electrons, leading to the emission of characteristic X-rays. These X-rays are detected and analysed to identify and quantify the elements present in the sample.

Modern SEM systems are equipped with field emission sources, advanced detectors, and automated software controls, enabling precise and reproducible measurements. However, as Goldstein et al. emphasize, meaningful results still depend on the operator's ability to correctly choose and understand imaging parameters such as accelerating voltage, working distance, and detector settings [30].

The morphological properties of untreated-WPL and treated-WPL were characterized using scanning electron microscopy (Phenom XL Desktop SEM), as shown in Figure 11**,** at an operating voltage of 15 kV. The surface of the samples was sputter-coated with platinum before SEM imaging to enhance the conductivity of the natural fibers.

Elemental analysis of the samples was conducted through energy-dispersive X-ray spectroscopy integrated with the SEM.

Fig. 11. SEM (Phenom XL) with EDS for surface morphology and elemental analysis.

3.3.2. Fourier Transform Infrared Spectroscopy

Fourier Transform Infrared (FTIR) Spectroscopy is a widely used analytical technique that identifies molecular structures based on the absorption of infrared radiation by chemical bonds. According to Stuart [31], when IR radiation interacts with a molecule, specific bond vibrations

absorb energy at characteristic frequencies, leading to a spectrum that reflects the presence of functional groups such as –OH, –CH, –COOH, or –Si–O.

FTIR spectra are typically recorded as plots of absorbance (or transmittance) versus wavenumber (cm^{-1}), producing a unique molecular fingerprint for each substance. This enables the qualitative analysis of chemical compositions and the monitoring of structural changes, particularly in organic and polymeric materials. The use of Fourier Transform algorithms allows rapid acquisition of high-resolution spectra across a broad spectral range, improving signal-to-noise ratios and reducing acquisition time compared to traditional dispersive IR methods.

FTIR spectroscopy (TENSOR 27 FTIR spectrometer, BRUKER) was employed to identify functional groups and confirm chemical changes in the treated-WPL. FTIR spectra were recorded in the 400–4000 cm^{-1} range, with a resolution of 4 cm^{-1} and 64 scans at room temperature. The instrument used for this analysis is shown in Figure 12.

Fig. 12. FTIR spectrometer (Bruker TENSOR 27) for functional group identification.

3.3.3. Thermogravimetric Analysis

Thermogravimetric Analysis (TGA) is a technique used to monitor the mass of a sample as it is subjected to a controlled temperature program over time. This method provides detailed insight into a material's thermal stability, composition, and degradation behavior. The sample is placed in a small pan or crucible, typically made of platinum or ceramic, and positioned on an ultra-sensitive microbalance inside a temperature-controlled furnace.

As the temperature increases, any mass loss associated with processes such as moisture evaporation, thermal decomposition, or volatilization is continuously recorded. The test is typically conducted under either an inert (e.g., nitrogen or argon) or oxidative (e.g., air or oxygen) atmosphere, depending on the purpose of the analysis.

The resulting TGA curve plots weight percentage against temperature or time, and key features such as onset degradation temperature (T_{Onset}), inflection points, and final residue provide valuable data about the physical and chemical changes occurring in the material. This technique is beneficial for characterizing complex systems such as polymer composites, biomass fillers, and thermoset resins, where multi-stage degradation occurs [32].

The thermal stability of the treated-WPL was assessed via thermogravimetric analysis using a TGA-SDTA 851 system (Mettler Toledo, ISO 9001 and 14001). Approximately 20 mg of sample was analysed under an argon atmosphere, with the thermal degradation profile recorded from 30 °C to 700 °C at a heating rate of 10 °C/min and a gas flow rate of 50 ml/min. The experimental setup used for this analysis is depicted in Figure 13.

Fig. 13. TGA analyzer (Mettler Toledo TGA-SDTA 851) for thermal degradation profiling.

3.3.4. Dynamic mechanical thermal analysis and Payne effect analysis

Dynamic Mechanical Thermal Analysis (DMTA) is a sensitive technique used to evaluate the viscoelastic behavior of polymeric materials as a function of temperature, frequency, or time. In DMTA, a sinusoidal stress (or strain) is applied to the sample, and the resulting strain (or stress) response is measured. This enables the calculation of the storage modulus (E′), which represents

the elastic or energy-storing component, and the loss modulus (E″), which reflects the viscous or energy-dissipating component. The ratio of these values gives tan δ (E″/E′), an indicator of damping behavior and transition regions such as the glass transition temperature (T_g).

The test can be performed in various deformation modes, including tension, bending, and shear, using fixtures like dual cantilever or three-point bending setups. The sensitivity of DMTA makes it especially suitable for detecting secondary transitions and evaluating the effects of fillers, plasticizers, and cross-linking in polymer composites. It is widely employed to analyze thermomechanical stability, dynamic stiffness, and damping capacity in both research and quality control environments.

The results obtained from DMTA are critical for understanding the temperature-dependent mechanical performance of materials, making it an essential tool for characterizing rubber composites and other viscoelastic systems [33].

In this study, DMTA was done in which the thermal properties of the rubber vulcanizates were determined using a dynamic mechanical analyzer (Anton Paar (MCR702E)), as shown in Figure 14, at a frequency of 1 Hz in tension mode. The temperature range employed was from –65 to 80 °C.

The storage shear modulus (G') and loss modulus (G") of the rubber compounds with curatives were evaluated by using an Anton Paar (MCR702E) at a temperature of 100 °C, frequency of 1 rad/s, and varying strains in the range of 0.01-100%. The parallel plate fixture was equipped with a serrated surface texture to prevent slipping. The Payne effect was taken as the difference in storage shear moduli at low strain (0.01%) and high strain (100%).

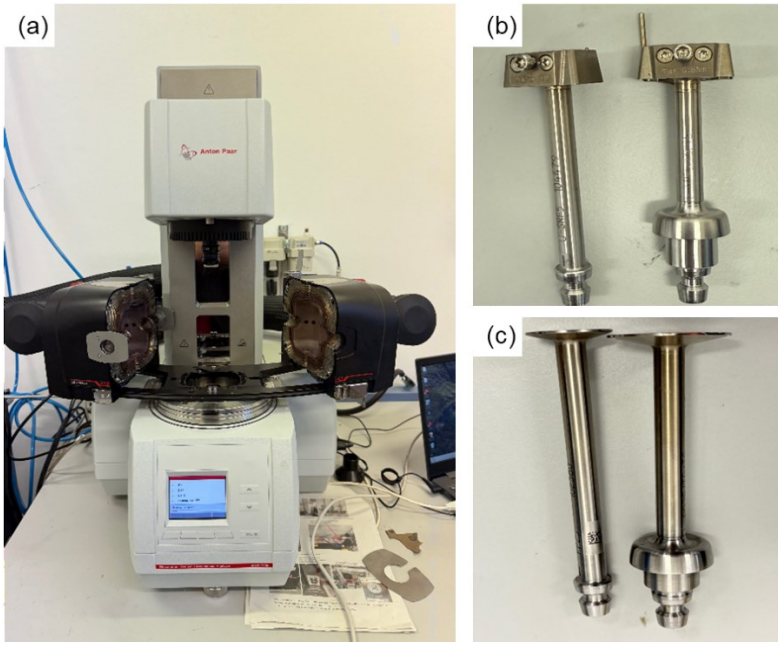

Fig. 14. a) DMTA (Anton Paar MCR702E) for viscoelastic and Payne effect analysis, b and c) clamps designed for specific sample geometries and test modes.

3.3.5. Mechanical properties

Mechanical properties are fundamental to evaluating how materials respond to external forces, and they play a critical role in determining the structural integrity and durability of polymer composites. In particular, tensile testing is one of the most widely used methods for characterizing mechanical performance. This test involves subjecting a standardized specimen to uniaxial tension until failure. The resulting stress–strain curve provides essential information such as Young's modulus, which indicates the stiffness of the material; tensile strength, which reflects the maximum stress the material can withstand before breaking; and elongation at break, which describes its ductility and ability to deform plastically without rupture.

In addition to tensile behavior, hardness is another critical mechanical characteristic, especially in elastomeric materials. Hardness measures a material's resistance to localized plastic deformation and is typically evaluated using a durometer. For rubber-like materials, the Shore A scale is commonly employed, where a standard indenter is pressed into the material's surface under defined conditions, and the resistance is recorded as a numerical value.

These mechanical tests are generally performed under controlled environmental conditions and standardized protocols, providing reliable data for comparing the effects of material composition, processing variables, or surface modifications. The combination of tensile and hardness testing

offers a comprehensive understanding of the composite's mechanical performance and its suitability for specific applications [34].

In this study, mechanical properties of the biofilled-rubber composites, such as tensile strength, elongation at break, and modulus, were determined using an INSTRON universal testing machine (Ulm, Germany) under ISO 527 (die type 5A). The test was carried out at 25 °C and a speed of 200 mm/min. The samples were cut from the vulcanized rubber sheets with a thickness of about 1 mm. An average of five replicate tests for each sample was recorded. The hardness, measured in Shore A, was determined using a durometer (HBA 100-0) based on ISO 868. An average value from five various positions was recorded for each specimen. The equipment used for these tests is shown in Figure 15.

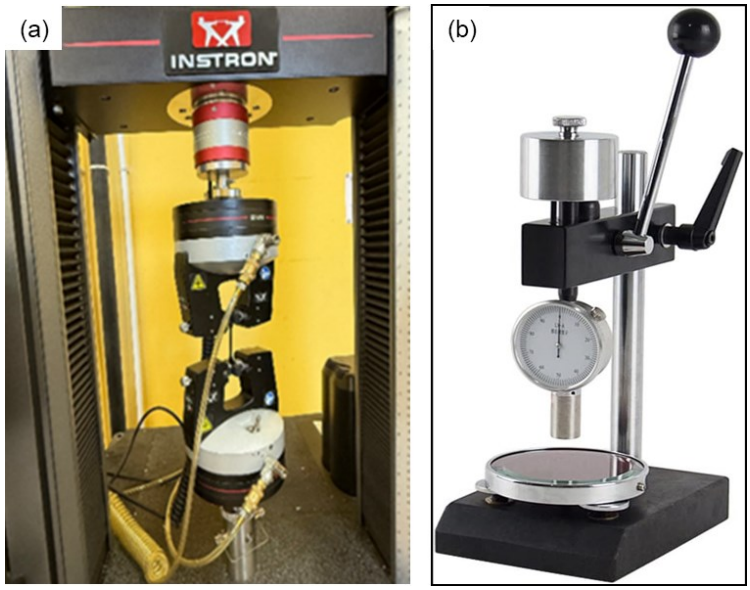

Fig. 15. (a) Universal testing machine (INSTRON), and (b) hardness Shore A durometer.

3.3.6. Swelling weight ratio

To evaluate the swelling behavior of NR/SBR composites reinforced with varying contents of 2%NaOH-WPL-2TESPT as biofiller, rectangular specimens with dimensions of 10 × 10 × 1 mm^3 were prepared from vulcanized samples. The initial dry weight of each specimen was accurately measured. The samples were then immersed in 40 ml of toluene and kept at room temperature for 72 hours. After the swelling period, the samples were gently removed from the solvent, and their surfaces were carefully blotted with soft tissue to eliminate excess toluene without applying

pressure. The swelling weight ratio (Q) of each specimen was calculated using the equation (1) [35]:

$$Q = \frac{W_S - W_0}{W_0} \quad (1)$$

where W_0 is the initial (dry) weight and W_S is the swollen weight of the specimen.

Result and discussion

4.1. Alkali treatment of WPL

4.1.1. Scanning Electron Microscope

The SEM images (Figure 16) illustrate the morphological changes in the WPL biofiller samples subjected to alkali treatment for various times of 1, 2, 3, 5, and 24 hours compared to the untreated WPL.

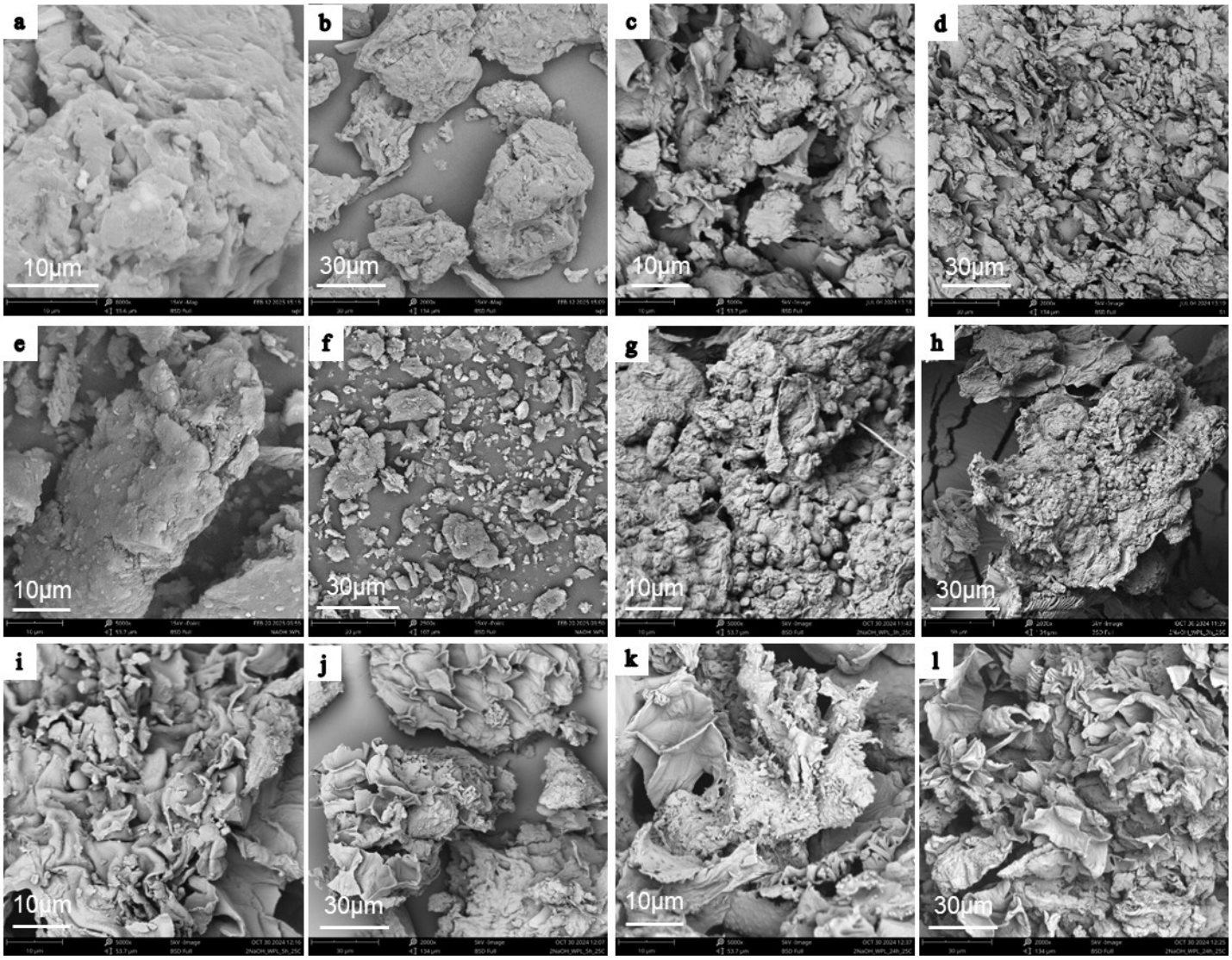

Fig. 16. SEM images of (a, b) untreated WPL, and alkali-treated WPL after various times : (c, d) after 1hr (e, f) after 2 hrs, (g, h) after 3 hrs, (i, j) after 5 hrs , and (k, l) after 24 hrs..

The untreated samples exhibit a compact and rough surface morphology, with fibers embedded within a dense matrix. After 1 hour of alkali treatment, initial signs of fiber exposure become apparent, accompanied by a slight increase in surface roughness and the formation of small pores, indicating partial removal of non-cellulosic components.

As the treatment duration extends to 5 hours, the fibers appear more distinct and separated, with a significant increase in surface roughness. Larger pores and cavities are evident, reflecting a more effective disruption of the lignin-hemicellulose. After 24 hours of alkali treatment, the samples exhibited a highly porous structure with extensively exposed and individualized fibers. The

substantial removal of non-cellulosic materials results in a rough and open morphology, highlighting the progressive impact of alkali treatment over time [29][36].

4.1.2. FTIR Spectroscopic

The IR spectra of untreated WPL and alkali-treated WPL (at various times) are presented in Figure 17.

The broad band in the range of 3000-3600 cm^{-1} corresponds to the stretching vibrations of hydroxyl groups (-OH). To ensure a reliable quantitative comparison, the spectra were normalized against the stable alkoxy group (C-O}) stretching band of the cellulose backbone at approximately 1028 cm^{-1}. In the alkali-treated samples, the intensity of this peak increases due to the disruption of the hydrogen bonding network within the cellulose structure, which frees more hydroxyl groups and enhances their exposure [37].As time increased, the absorbance in this range decreased. Moreover, alkali treatment breaks down hydroxyl groups, which react with NaOH and exit the fiber structure. The remaining molecules form fibre–cell–O–Na bonds, reducing hydrophilic properties and improving moisture resistance. This process also removes portions of hemicellulose and lignin [7], [10][27].

$$\text{Fibre-cell-OH} + \text{NaOH} \longrightarrow \text{Fibre cell-O-Na}^{+} + H_2O + \text{impurities}$$

The peaks observed at 2800–2950 cm^{-1} are associated with the C–H stretching vibration of methyl and methylene groups in Cellulose and hemicellulose [36][27].

The sharp peak at approximately 1743 cm^{-1}, attributed to ester carbonyl groups (C=O stretching) in hemicellulose [10][36][27], diminishes significantly after alkali treatment. This reduction indicates the effective removal of hemicellulose, which is one of the primary objectives of the treatment. The peaks at **1607 cm^{-1}** and 1513 cm^{-1} are typically attributed to **C=C stretching vibrations in the aromatic rings of lignin**. A decrease in the intensity of these peaks after alkali treatment provides insight into removing lignin and other related structural changes [7][36]. The peak at 1444 cm^{-1} corresponds to the bending vibration of CH_2 groups in the crystalline structure of Cellulose [36]. The peaks at 1372 cm^{-1} and 1318 cm^{-1} are associated with the C–OH stretching vibration and the C–O stretching vibrations, respectively, which are characteristic of the crystalline structure of Cellulose [7][36]. The absorption peak at ~1230 cm^{-1} is attributed to C–O stretching vibrations in hemicellulose and lignin. In the case of alkaline-treated WPL, a notable reduction in this peak suggests that lignin and hemicellulose removal occur during the alkaline treatment

process. The peak at 1028 cm^{-1} is attributed to the presence of the alkoxy group (C-O) in Cellulose, specifically related to the vibrations of hydroxyl (-OH) and ester (-COO-) groups [29]. The respective band positions of the various samples are listed in Table 3.

Table 3. Characteristic peaks and corresponding functional groups in FTIR analysis.

Wave number cm^{-1}	**Peak assignments**
3000-3600	O–H stretching vibration
1743	C=O (Ester Carbonyl Group) in hemicellulose
1607 and 1513	C=C **vibrations in the aromatic rings of lignin**
1444	CH_2 groups in the crystalline structure of Cellulose
1372	C–OH stretching vibration in the crystalline structure of Cellulose
1318	The C–O stretching vibration in the crystalline structure of Cellulose
1230	C–O stretching vibrations in hemicelluloses and lignin
1028	Alkoxy group (C-O) in Cellulose

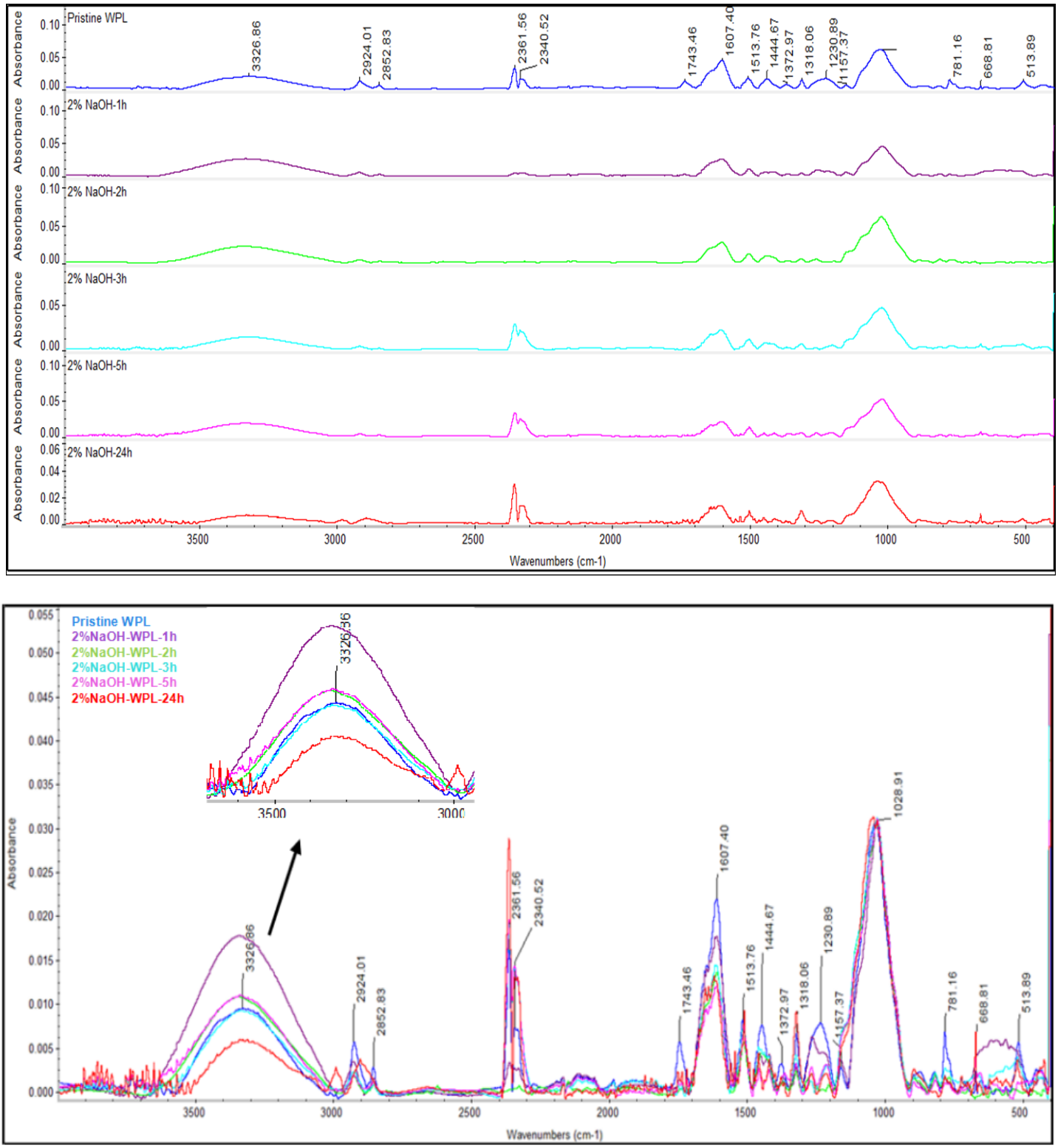

Fig. 17. FTIR spectra of WPL before and after the alkali treatment at various times in the range of 400-4000 cm^{-1} (Normalized).

4.1.3. TGA analysis

TGA analysis of alkali-treated WPL samples provides insights into the samples' thermal stability and decomposition behavior at different treatment durations. The TGA and DTG curves (first derivative of the TGA curve) for unmodified WPL and alkali-treated WPL are presented in Figure 18a and 18b, respectively. Furthermore, the thermal data derived from the TG/DTG curves for both unmodified WPL and NaOH-treated WPL are summarized in Table 4.

The first weight loss (1st Step) occurred at a temperature up to 120 °C, attributed to the evaporation of water from the fibers [29]. The weight loss percentages were **7.4%, 5.6%, 5.2%, 6.7%, 5.6%,** and **3.9%** for pristine WPL and alkali-treated WPL for 1, 2, **3, 5, and 24 hours, respectively**. The decreasing trend in water loss indicates that prolonged alkali treatment effectively reduces moisture retention.

The second stage occurred in the temperature range of 200-600 °C, attributed to the decomposition of the lignocellulosic material such as Cellulose, hemicellulose, and lignin [38]. Compared with the unmodified WPL, the alkali treatment increases T_{onset} for all treated samples. This can be explained by the reduction in the concentration of extractives, hemicellulose, and lignin, which was caused by the alkali treatment. The extractives include pectin, waxes, and natural resins, which are compounds that have degradation temperatures lower than cellulose. Alkali treatment increases the average size of the fibers, decreasing the superficial area, so that a higher specific energy is needed to degrade the fibers [29]. However, there was a decrease in the maximum degradation rate (T_{max}) after alkali treatment. The final stage of degradation showed the removal of lignin and other impurities. The residue after filler degradation was the highest for pristine WPL. After alkali treatment, the residue initially decreased due to the removal of lignin, but then increased again for longer times. This subsequent increase is attributed to the significant reduction of hemicellulose during prolonged alkali exposure, which promotes the formation of a stable lignin-cellulose complex and condensed carbon rings, thereby enhancing the residual char formation. Among the constituents of lignocellulosic materials during pyrolysis, lignin has the highest proportion of solid residue [7][27][39][40].

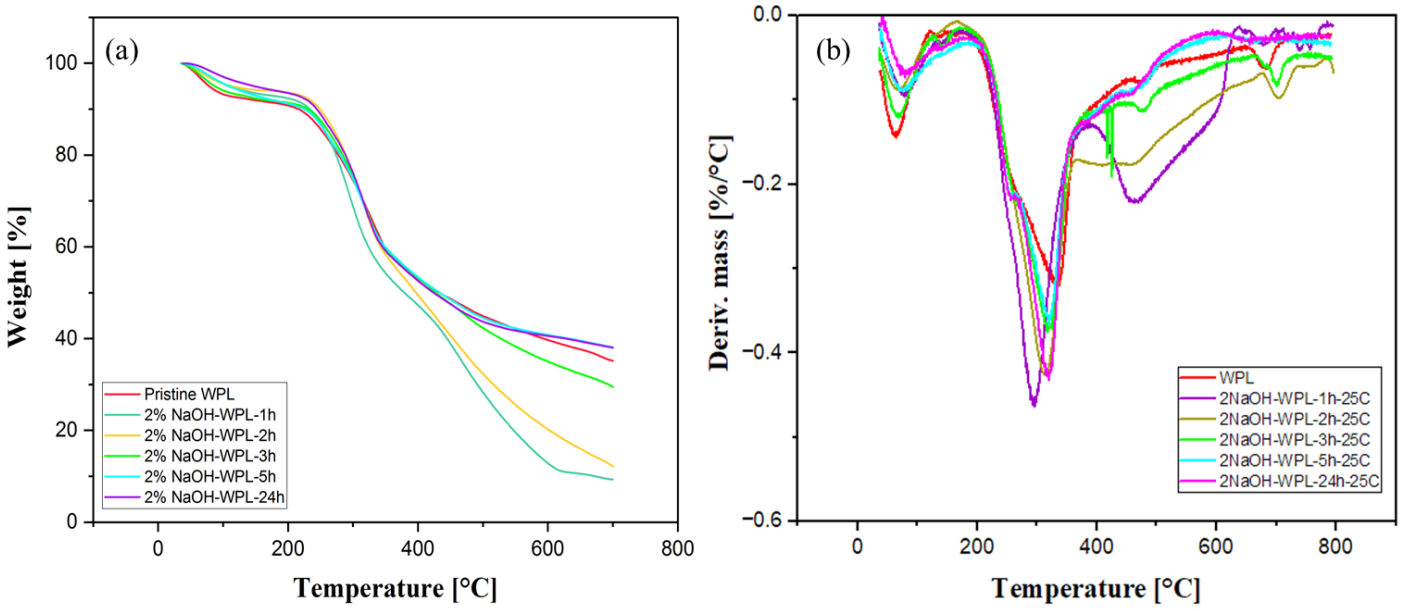

Fig. 18. (a) The TGA and (b) DTG curves of untreated and alkali-treated WPL.

Table 4. Thermal data from TGA/DTG curves of treated and untreated WPL.

Sample	1st Step (wt.%)	T_{Onset} (°C)	T_{max} (°C)	R700(%)
Pristine WPL	7.4	226	332	35.3
2%NaOH-WPL-1h	5.6	232.5	296	9.4
2%NaOH-WPL-2h	5.2	236.6	314	12.2
2%NaOH-WPL-3h	6.7	238.3	317	29.8
2%NaOH-WPL-5h	5.6	235.8	320	38.2
2%NaOH-WPL-24h	3.9	232.9	318	38.0

The 2%NaOH-WPL-2h was chosen based on FTIR and TGA results. FTIR analysis confirmed a substantial reduction in hemicellulose and lignin content. Furthermore, TGA results demonstrated enhanced thermal stability, with a higher onset temperature (T_{Onset} = 236.6 °C), lower moisture retention (5.2 wt%), and a reduced residual mass at 700 °C (R700 = 12.2%), indicating more effective removal of non-cellulosic components.

An SEM-EDX study was conducted to further validate these results, offering additional proof of the compositional and structural alterations caused by the alkali treatment.

4.1.4. SEM/EDX analysis

Figures 19 and 20 show SEM micrographs and the elemental mapping images of untreated WPL and 2% NaOH-WPL-2h.

As can be seen in Figure 19, the untreated WPL sample exhibits a compact and dense surface morphology, with an irregular texture and embedded particles.

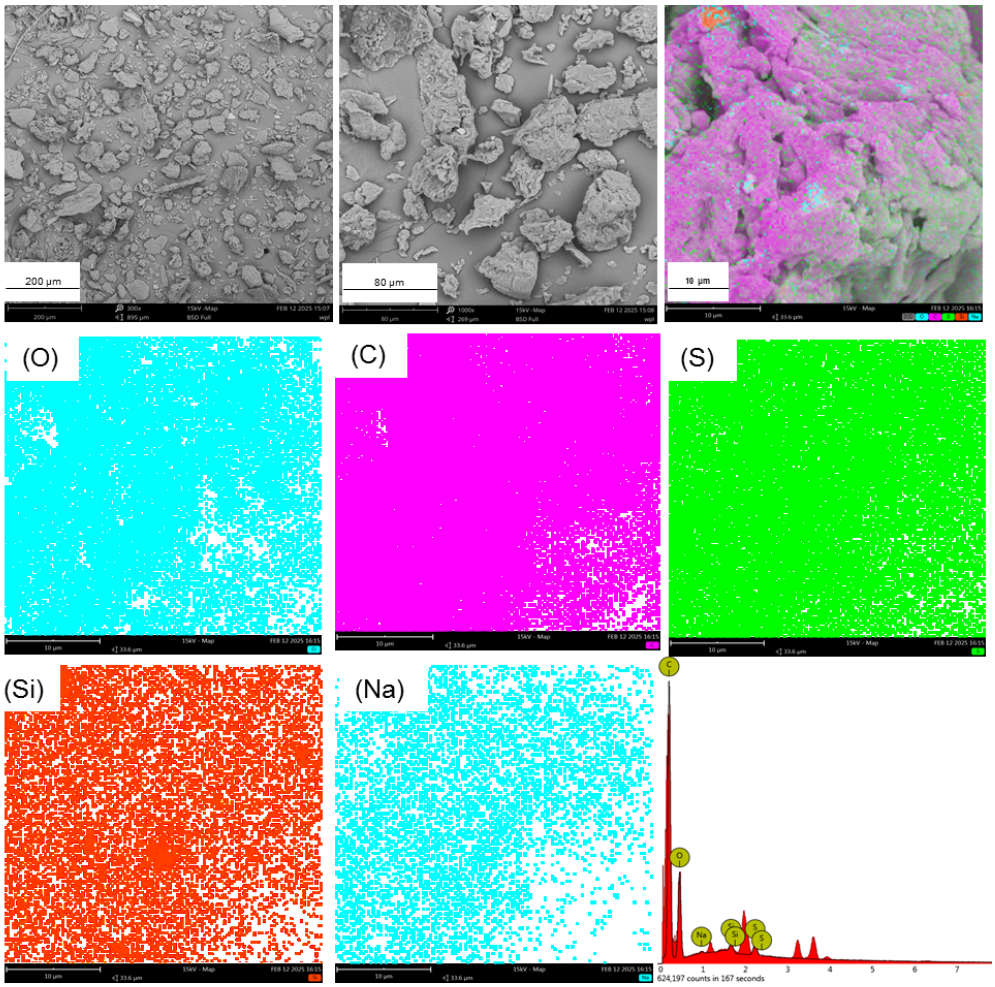

Fig. 19. SEM images, EDX spectrum, and element mapping image of untreated WPL.

Figure 20 illustrates the morphological changes observed after 2 hours of alkali treatment, where the surface becomes noticeably rougher with increased porosity and the formation of small voids. These structural modifications suggest the partial removal of hemicellulose and lignin, resulting in a more porous and reactive surface.

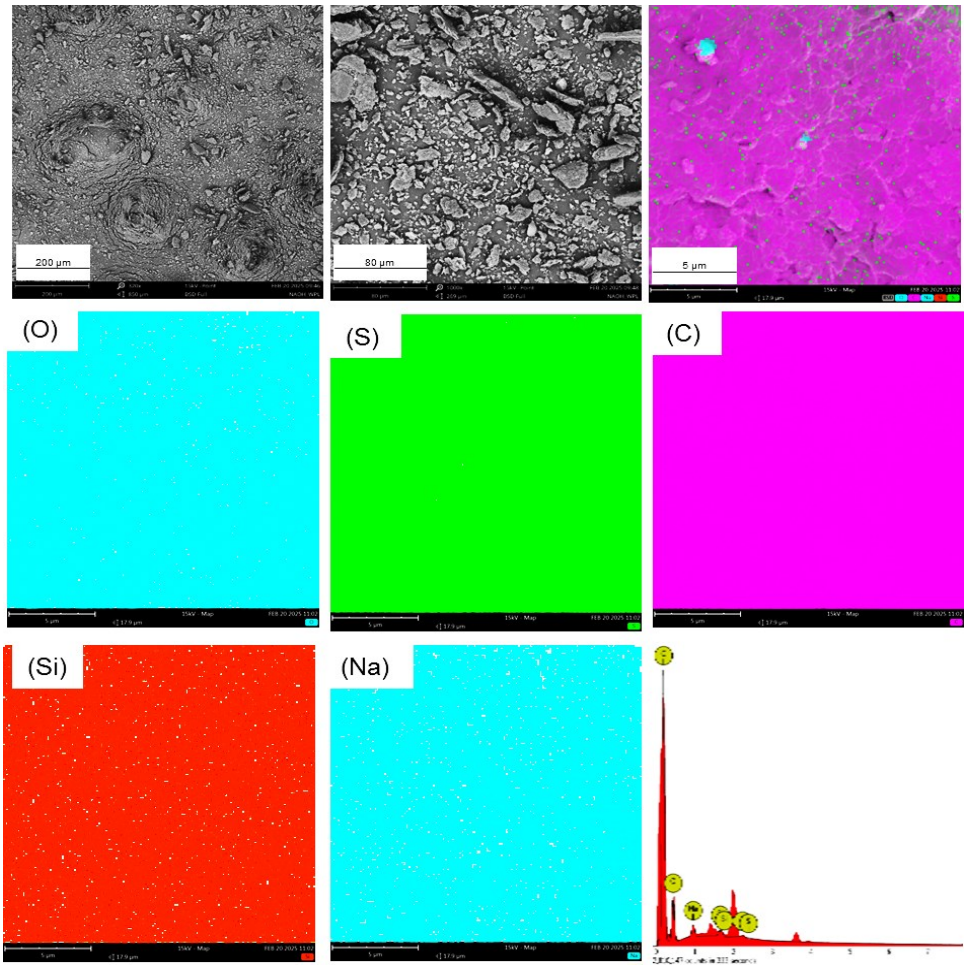

Fig. 20. SEM images, EDX spectrum, and element mapping image of 2%NaOH-WPL-2h.

Table 5 presents the EDX analysis of the elemental composition of the untreated-WPL and 2%NaOH-WPL-2h sample, confirming carbon (C) and oxygen (O) as the dominant elements, which are characteristic of lignocellulosic materials. The presence of sulfur (S) and silicon (Si) in the untreated WPL sample may be attributed to residual inorganic impurities derived from the raw material or processing additives. Alkali treatment of WPL resulted in a decrease in oxygen content and an increase in carbon content, leading to a lower O/C ratio [41]. Additionally, the increase in sodium (Na) content after alkali treatment further confirms the impact of the chemical modification, contributing to the structural changes observed.

Table 5. Elemental analysis (EDX) of untreated WPL and 2%NaOH-WPL-2h.

Element	Untreated WPL (wt. %)	2%NaOH-WPL (wt. %)
Oxygen (O)	67.3	54
Carbon (C)	26.1	34
Sulfur (S)	3.5	0.5
Silicon (Si)	1.8	2
Sodium (Na)	1.3	9.4

4.2. Combined NaOH-Silane treatment

4.2.1. FTIR measurements

The IR spectra of NaOH-TESPT-treated WPL samples are presented in Figure 21. In addition, the spectrum of pure TESPT is shown for comparison.

The FTIR spectrum of pure TESPT exhibits characteristic peaks confirming its structural composition. The absorption bands at 2972 cm^{-1}, 2923 cm^{-1}, and 2884 cm^{-1} correspond to $–CH_2$ and $–CH_3$ stretching vibrations of silane [42]. The IR absorption band near 1200 cm^{-1} has been attributed to C–O–Si bonds [42].In pure TESPT silane, this band was observed at 1242 cm^{-1} [42]. The bands at 1099.69 cm^{-1} and 1074.92 cm^{-1} correspond to Si–O–Si stretching in silica structure and CH3CH2-O groups of silanes [42]. The band at 957 cm^{-1} and 784 cm^{-1} correspond to the stretching of Si-O in silanol and the deformation of Si-OH, respectively. The peak at 478 cm^{-1} is attributed to Si-O-Si bending [42].

In the spectrum of treated-WPL, the broad and strong peak around 3326 cm^{-1} corresponds to the O-H stretching vibrations. Upon treatment with TESPT, this peak shows a noticeable decrease in intensity with respect to 2%NaOH-WPL-2h, indicating the occurrence of bonding between alkoxysilanes and the fibers. This reduction showed that the silanization process decreases the hydrophilicity of the WPL, enhancing its compatibility with hydrophobic matrices [43][3][44]. After silanization, a new peak appeared in TESPT-treated samples around 2920 cm^{-1}, attributed to -CH2 and -CH3 stretching of TESPT molecules. In addition, the spectrum of 2%NaOH-WPL-2TESPT and 2%NaOH-WPL-10TESPT samples exhibited an additional small shoulder around 2972 $cm^{-1,}$ related to -CH2 and -CH3 stretching of TESPT molecules. Therefore, IR absorption bands at around 2920 cm^{-1} and 2972 cm^{-1} in the TESPT-treated WPL samples confirm that the fiber surface was successfully modified through silane adsorption.

However, some peaks related to pure TESPT silane overlap with the intense peak from Cellulose in the same spectral region and are challenging to see. Similarly, the characteristic Si–O–Si vibrations are masked by the strong C–O stretching absorption around 1098 cm^{-1}, as previously observed in studies on silane-treated cellulosic materials [42][45][36]. For this reason, further analysis is provided through SEM-EDX and TGA analysis to confirm silane attachment on the surface of the alkali-treated WPL. The key absorption bands, along with their corresponding wave numbers and functional group assignments, are summarized in Table 6.

Table 6. Characteristic peaks and corresponding functional groups in FTIR analysis.

Wave number cm^{-1}	**Peak assignments**
3000-3600	Stretching vibrations of the O-H groups in the Cellulose
2800-3000	C–H stretching vibration from the -CH2 groups in Cellulose
2972, 2923, 2884	$–CH_2$ and $–CH_3$ stretching vibrations of TESPT silane
1440	C-H deformation (lignin) and CH2 symmetric bending (Cellulose)
1242	Si-O-C asymmetric stretching, characteristic of silanes
1099 and 1074	Si–O–Si stretching in silica structure and CH_3CH_2–O groups of silanes
957	Si–O stretching in silanol
784	deformation of Si-OH
478	Si–O–Si bending
1743	C=O (Ester Carbonyl Group) in hemicellulose
1607 and 1513	C=C **vibrations in the aromatic rings of lignin**
1230	C–O stretching vibrations in hemicelluloses and lignin

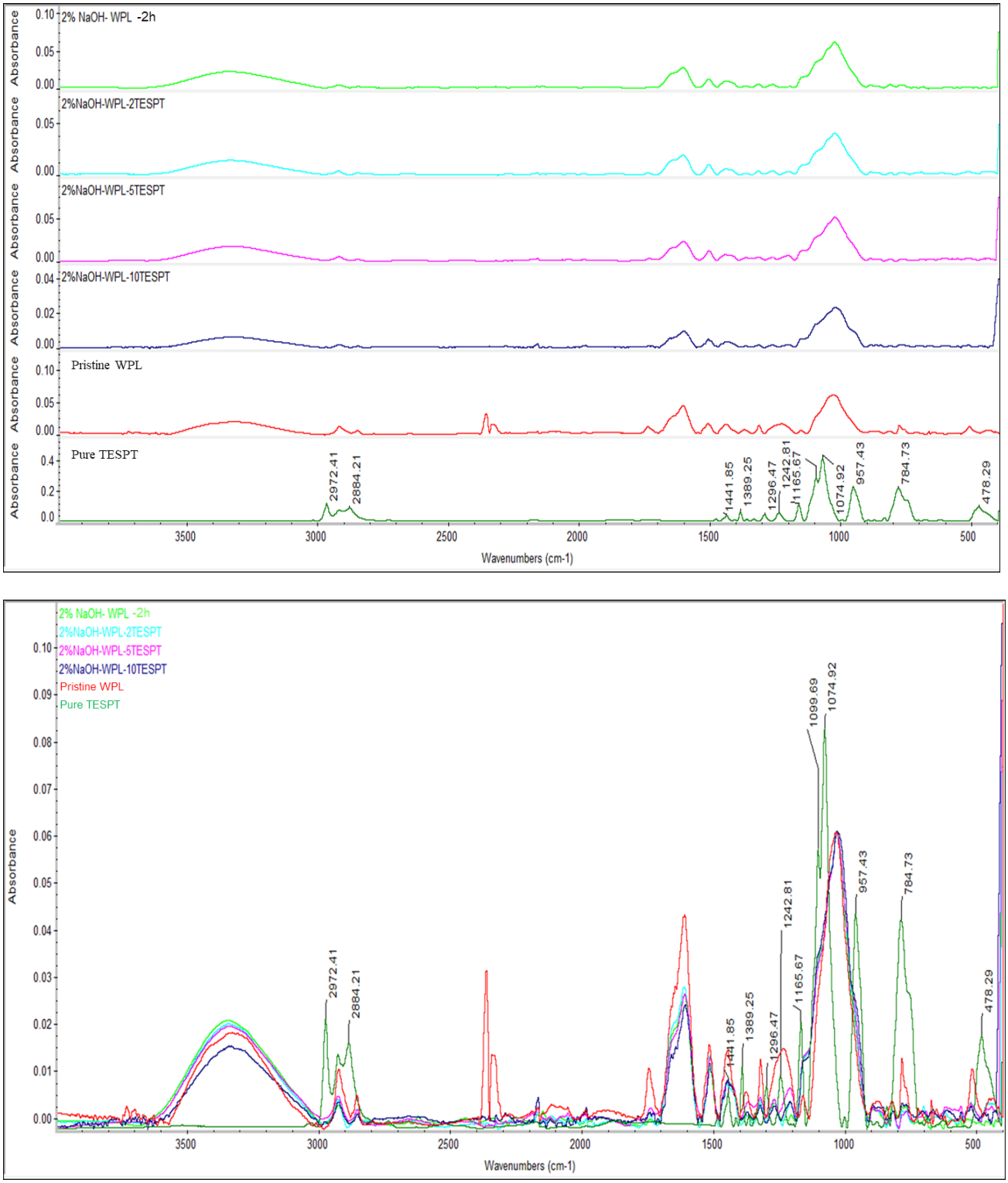

Fig. 21. FTIR spectra of untreated-WPL, alkali-treated WPL, and combined alkali-silane-treated WPL at various TESPT concentrations (Normalized).

4.2.2. SEM analysis

The SEM-EDX analysis was performed on 2%NaOH-TESPT-WPL samples (with various silane concentrations) to evaluate the effect of silane treatment on the morphology and elemental composition of the samples.

Figures 22, 23, and 24 present SEM images and elemental mapping of 2%NaOH-WPL-2TESPT, 2%NaOH-WPL-5TESPT, and 2%NaOH-WPL-10TESPT, respectively, illustrating the morphological changes following silane treatment. The structure undergoes significant modifications, becoming more stratified and exfoliated, with reduced compactness and improved dispersion. The lignocellulosic matrix appears disrupted and layered, likely due to the removal of hemicellulose and the combined effects of alkali and silane treatments.

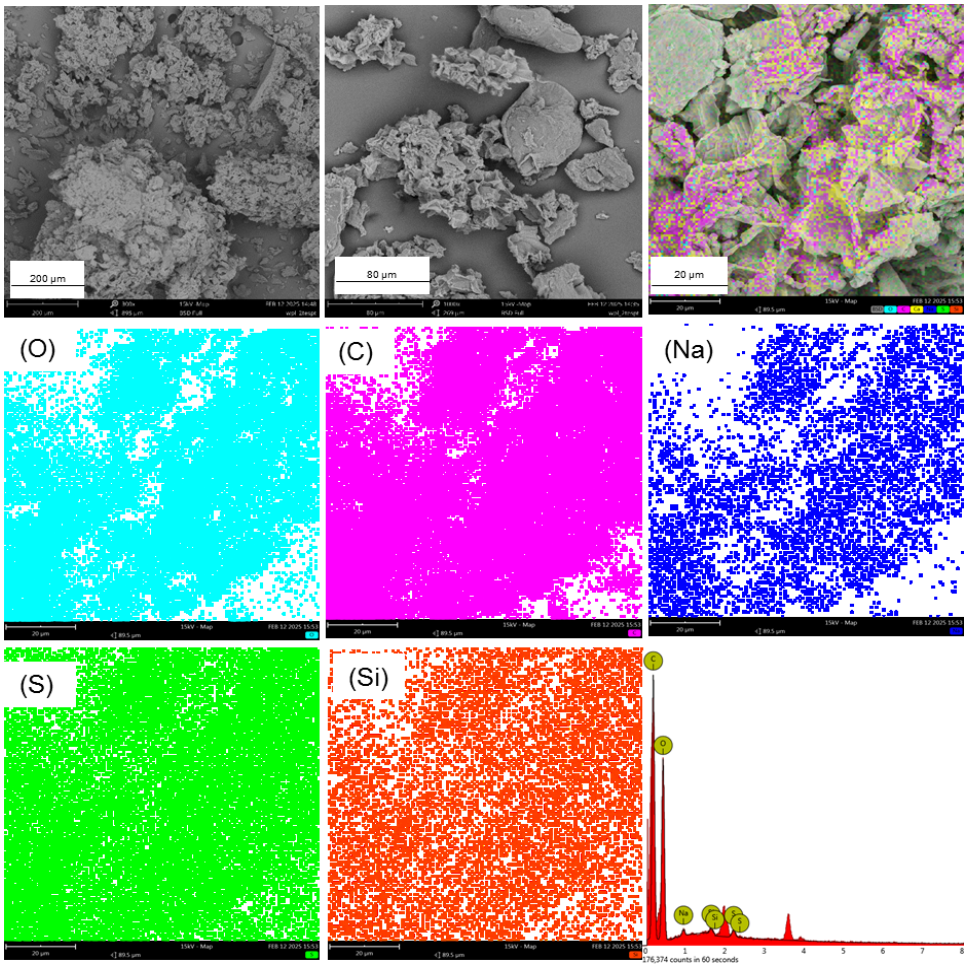

Fig. 22. SEM images, EDX spectrum, and element mapping image of 2%NaOH-WPL-2TESPT.

Additionally, an increase in surface roughness is observed, consistent with previous studies on silane-treated lignocellulosic materials [3][8][43][16]. These structural alterations result in a larger

surface area, enhancing interfacial interactions with polymer matrices and improving overall filler compatibility.

The elemental mapping images in Figure 22 show a uniform distribution of carbon and oxygen in the 2%NaOH-WPL-2TESPT sample, reflecting the lignocellulosic composition of WPL. Moreover, the Si and S elements are well-dispersed across the surface without any visible clustering, suggesting a homogeneous silane grafting process. This even distribution enhances the interaction between TESPT and the WPL matrix, ensuring a more stable modification.

In contrast, in the 2%NaOH-WPL-5TESPT sample (Figure 23), while Si and S remain relatively well-distributed, some localized accumulations begin to appear. This suggests that at a higher TESPT concentration, silane molecules start to cluster in specific regions rather than dispersing evenly.

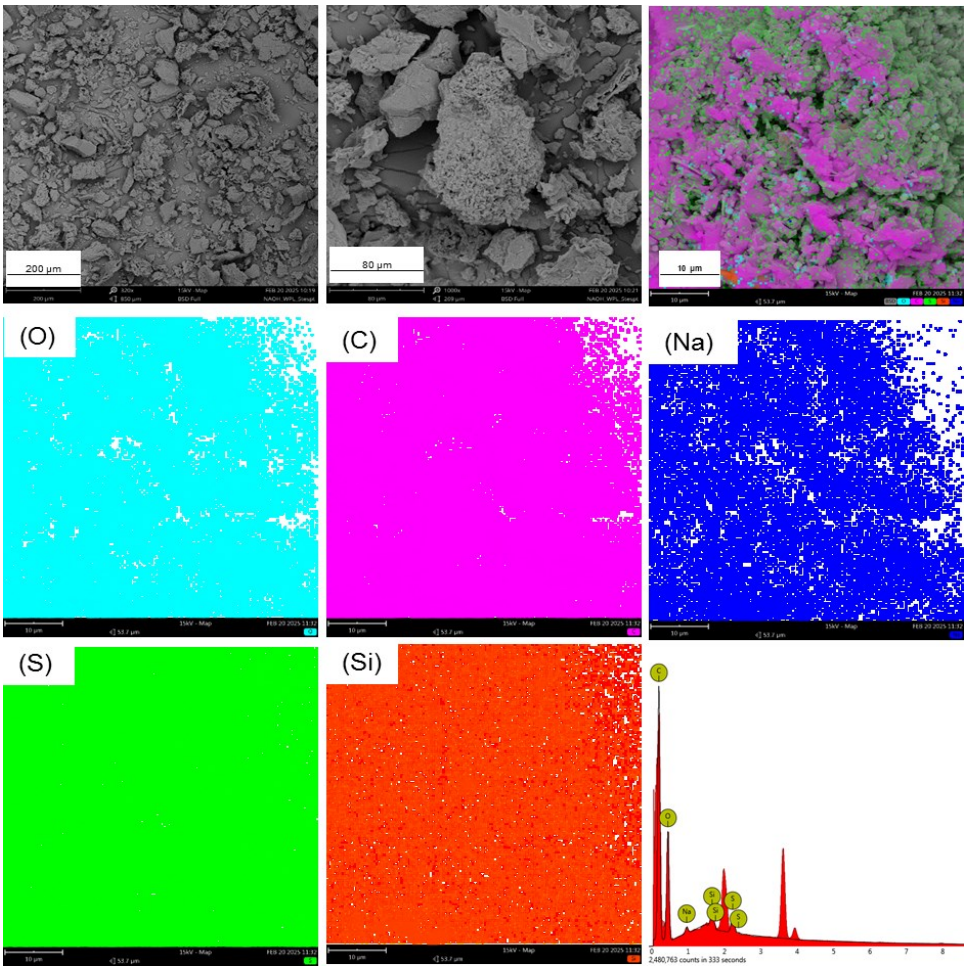

Fig. 23. SEM images, EDX spectrum, and element mapping image of 2%NaOH-WPL-5TESPT.

The 2%NaOH-WPL-10TESPT sample (Figure 24) exhibits clear agglomeration of Si and S, particularly in certain areas, indicating oversaturation of silane molecules on the WPL surface. In contrast to the lower TESPT concentrations, where silicon and sulfur were more evenly distributed, this sample exhibits noticeable clustering, which may reduce the uniformity and effectiveness of the silane treatment.

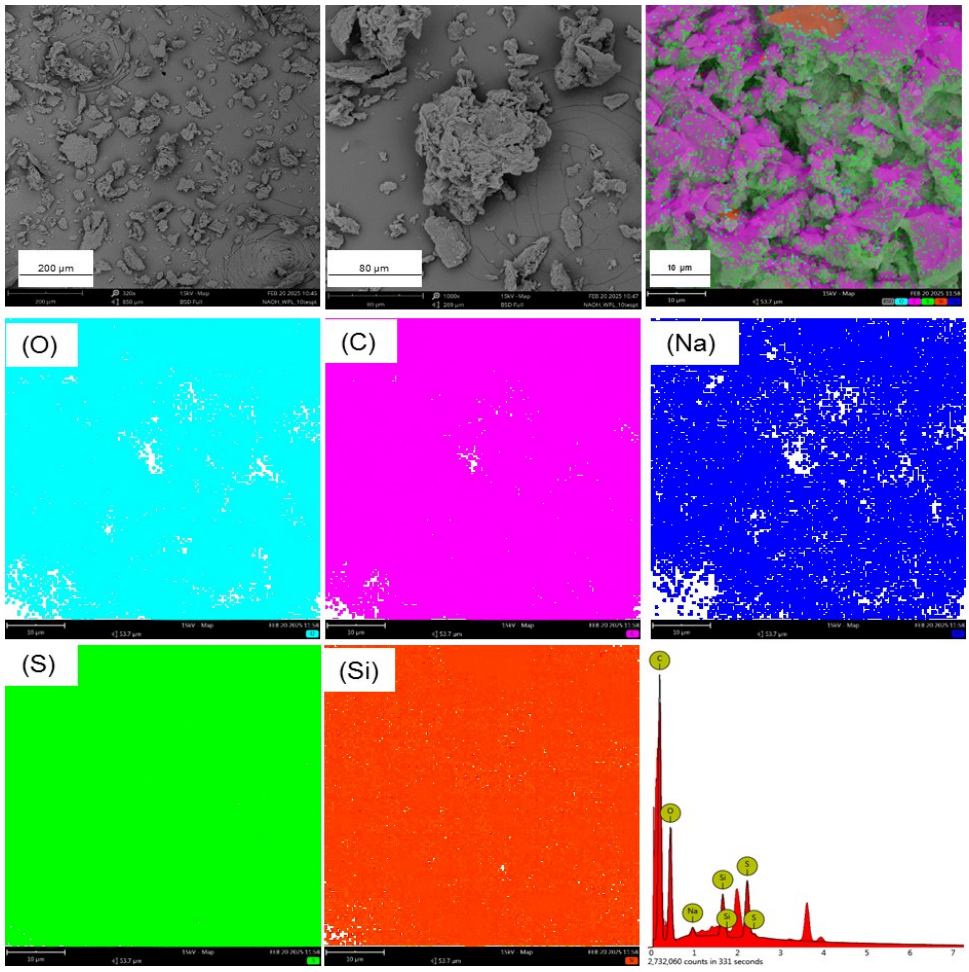

Fig. 24. SEM images, EDX spectrum, and element mapping image of 2%NaOH-WPL-10TESPT.

4.2.3. TGA Analysis

Figure 25a illustrates the TGA curves for untreated WPL, 2%NaOH-WPL-2h, and combined alkali-silane-WPL samples. The DTG curves reveal distinct thermal degradation stages (Figure 25b). The thermal data derived from the TG/DTG curves for both untreated WPL and treated WPL are summarized in Table 8.

The first stage, occurring between 50–120 °C, corresponds to the evaporation of moisture within the WPL. Pristine WPL exhibits the highest moisture loss (7.4 wt%), indicating its strong

hydrophilic nature. The smallest weight loss during this stage was observed in NaOH-TESPT-treated samples, indicating enhanced hydrophobicity [3][16].

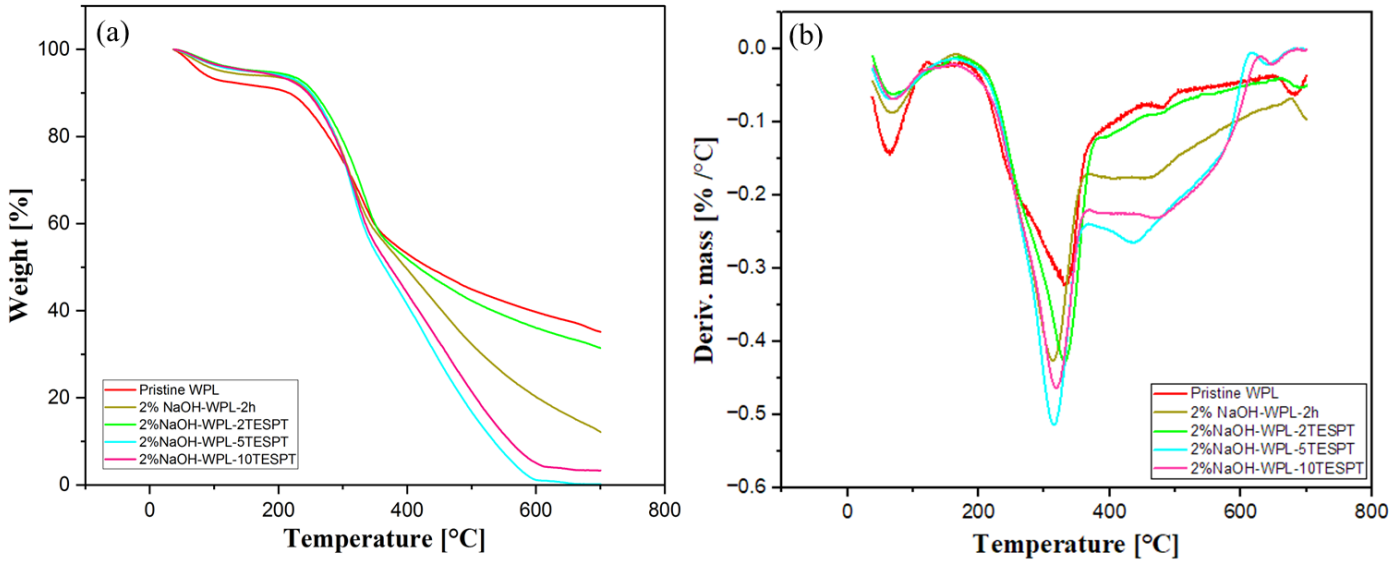

Fig. 25. a) TGA, and b) DTG curves of Pristine WPL, alkali-treated WPL, and combined alkali-TESPT-treated WPL samples.

In comparison with the untreated WPL and alkali-treated WPL, the T_{onset} improves after the combination of alkali and silane treatment, confirming the positive impact of silane modification on thermal stability of the samples [44][16]. The surface modification with TESPT silane increases the T_{onset} by 25 °C in the presence of 2 wt% TESPT, 20 °C for 5 wt% TESPT, and 22 °C for 10 wt% TESPT (Table 8). As can be seen in Figure 19b, pristine WPL exhibits T_{max} at 332 °C, whereas 2%NaOH-WPL-2h shows a reduction to 315 °C, due to changes in the lignocellulosic matrix after the removal of hemicellulose. However, concerning alkali-treated WPL, TESPT treatment leads to an increase in T_{max}, particularly in the 2%NaOH-WPL-2TESPT, where T_{max} rises to about 333 °C. This improvement could be attributed to the formation of a siloxane layer on the WPL surface [8]. Nonetheless, T_{max} slightly decreased to 312 °C for the 5 wt% TESPT sample, but increased again to 321 °C for the 10 wt% TESPT sample.

At elevated temperatures (700 °C), the remaining char residue provides insight into the thermal resistance of the treated samples. The residue after filler degradation was the highest for pristine WPL. Following silane treatment, samples display differing residual weights, with 2%NaOH-WPL-2TESPT demonstrating the most stable residue, which could be due to the presence of an

additional residue after the degradation of the modifier. In samples with less silane, more organic matter burns off completely, leaving behind a higher percentage of inorganic material [8][3][46].

Table 7. Thermal data from TGA/DTG curves of untreated WPL and treated-WPL.

Sample	1st Step (wt.%)	T_{Onset} (°C)	T_{max} (°C)	R700 (%)
Pristine WPL	7.4	226	332	35.3
2%NaOH-WPL-2h	5.2	237	315	12.2
2%NaOH-WPL-2TESPT	3.9	251	333	31.4
2%NaOH-WPL-5TESPT	4.3	246	312	0.2
2%NaOH-WPL-10TESPT	4	248	321	3.3

Furthermore, the amount of TESPT grafted onto 2%NaOH-WPL was quantified based on TGA analysis by calculating the weight loss between 150 °C and 380 °C using the equations (2) [45][46]:

$$\text{Amount of silane grafting (mg g}^{-1}) = 1000 \times W_{150-380} \quad (2)$$

Where $W_{150-380}$ represents the mass loss percentage in this temperature range. The molecular weight of TESPT (**538.95 g mol⁻¹**) was subsequently used to quantify the grafted silane content in mmol. g^{-1} (according to equation 3):

$$\text{Amount of silane grafting (mmol/g)} = \frac{\text{Amount of silane grafting}}{M} \quad (3)$$

The calculated values for 2%NaOH-WPL-TESPT samples are summarized in Table 8. The 2%NaOH-WPL-2TESPT exhibited a grafted silane content of 0.76 mmol g^{-1}, while increasing TESPT concentration to 5 wt% and 10 wt% resulted in higher silane grafting values of 0.91 mmol g^{-1} and 0.87 mmol g^{-1}, respectively, as confirmed by EDX analysis (Table 9). These results confirm that TESPT was successfully grafted onto the surface of alkali-treated WPL.

Table 8. Silane grafting content of 2%NaOH-WPL-TESPT samples.

Sample	W_{150} (wt%)	W_{380} (wt%)	Grafted silane (mmol. g^{-1})
2%NaOH-WPL-2TESPT	95.3	54.2	0.76
2%NaOH-WPL-5TESPT	95.1	46.1	0.91
2%NaOH-WPL-10TESPT	95.2	48.4	0.87

4.3. Surface-modified biofiller-reinforced Rubber composite

4.3.1. Mechanical properties

Figure 26 illustrates the mechanical properties of NR/SBR composites reinforced with 2%NaOH-WPL-2TESPT, including tensile strength, elongation at break, modulus, and hardness as a function of filler loading. The corresponding numerical values are reported in Table 10.

The control sample exhibited a tensile strength of 11 MPa. Interestingly, in the presence of 10 phr treated-WPL, the tensile strength was restored to 11 MPa, equivalent to that of the control sample. This indicates that 10 phr is the optimal filler loading, improving interfacial bonding. Silane functional groups attached to the surface of WPL acted as compatibilizers and effectively enhanced the interaction between the treated-WPL and the matrix. Moreover, the sulfur atoms present in the TESPT groups attached to the WPL facilitated cross-linking with rubber molecules. However, with the addition of 5, 20, and 30 phr of 2%NaOH-WPL-2TESPT, tensile strength decreased to approximately 8.8 MPa, 8.8 MPa, and 8.6 MPa, respectively. The presence of WPL disrupts the natural rubber chain arrangement, reducing strain-induced crystallization and lowering tensile strength [7]. This reduction can be attributed to filler agglomeration and poor distribution within the matrix, resulting in poor interaction and bonding between filler and matrix and reduced mechanical integrity [3][7].

The control sample exhibited the highest elongation value of 451%, indicating high elasticity. The incorporation of 5 phr treated-WPL resulted in a sharp decrease in elongation to 284 %, suggesting that rigid filler particles restricted the extensibility of the rubber matrix, thereby reducing flexibility. However, at 10 phr, elongation improved to 398 %, which indicates enhanced filler dispersion and improved interfacial bonding. At higher filler contents (20 and 30 phr), elongation fluctuated, reaching 348 % and 428 %, respectively. The increase in elongation in the presence of 30 phr of filler may be attributed to weak stress transfer within the composite, which allows the material to undergo higher deformation before failure [7][47].

Table 9. Mechanical properties of reinforced-NR/SBR composites with varying amounts of 2%NaOH-WPL-2TESPT as biofiller

Samples	Tensile strength (MPa)	Elongation at break (%)	Modulus (MPa)	Hardness (Shore A)
100 CB	11± 0.4	451±32	46.8±3.5	68±3
2%NaOH-5WPL-2TESPT	8.8± 1.2	284±20	51.1±3	69±2
2%NaOH-10WPL-2TESPT	11± 0.6	398±30	51.5±4.9	69±2
2%NaOH-20WPL-2TESPT	8.8± 0.6	348±37	58.5±4.4	70±2
2%NaOH-30WPL-2TESPT	8.6± 0.5	428±33	50.8±2.8	69±2

The Young's modulus, which represents the stiffness of the material, increased with loading treated-WPL up to 20 phr. The modulus in the control sample was 46.8 MPa. With the incorporation of 5 and 10 phr treated-WPL, the modulus increased to 51.1 MPa and 51.5 MPa, respectively, reflecting improved rigidity [47]. This trend continued, reaching a maximum of 58.5 MPa for 20 phr treated-WPL, indicating that the composite became stiffer with the addition of more filler [3][47]. However, at 30 phr, the modulus slightly decreased to 50.8 MPa, still higher than the control sample, which could be attributed to poor filler dispersion or the formation of weak interfacial regions, reducing the material's ability to transfer stress efficiently.

A slight increase in hardness with treated-WPL loading is due to the presence of rigid filler particles and a possible increase in crosslink density [3][47].

Considering the standard deviations in the mechanical properties, up to 30 phr of the treated-WPL can be used to partially replace carbon black without substantial variation, indicating acceptable performance consistency.

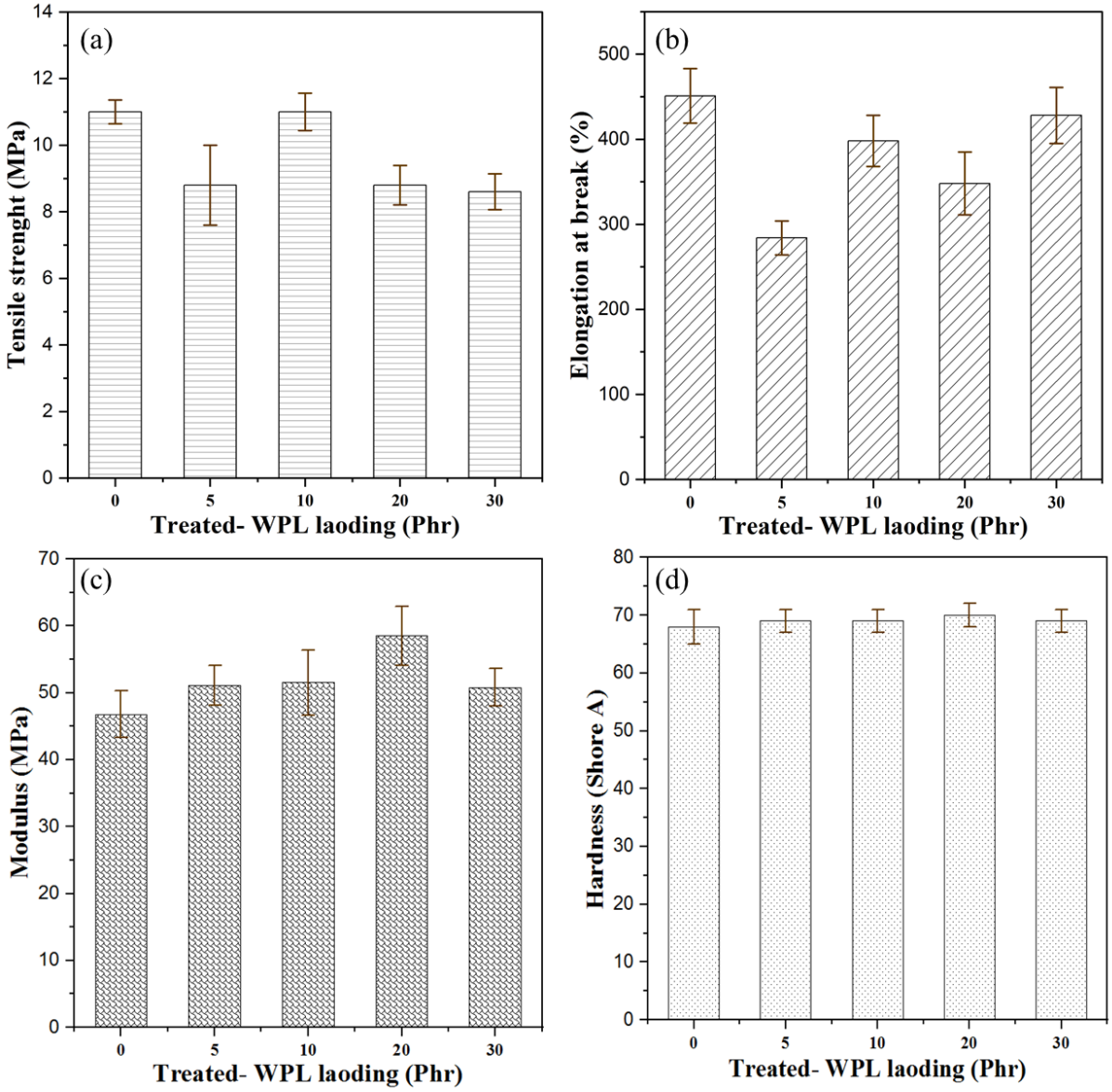

Fig. 26. Mechanical properties of NR/SBR composites reinforced with 2%NaOH-WPL-2TESPT at different filler loadings : (a) Tensile strength, (b) Elongation at break, (c) Modulus, and (d).

4.3.2. DMTA

The dynamic mechanical thermal behavior of NR/SBR composites containing CB/2%NaOH-WPL-2TESPT (at different filler loadings) was analyzed using E' values and loss factor (tan δ) as a function of temperature. The obtained results are demonstrated in Figure 27. Besides, Table 11 summarizes the numerical values of maximum tan δ (tan δ_{max}) and glass transition temperature (T_g) for each sample.

Figure 27a illustrates the variation of E' with temperature in the range of -65 ℃ to 90 ℃. Below T_g, the control sample containing only CB exhibits the highest E', confirming strong filler-filler interactions that dominate when polymer chain mobility is restricted. Upon incorporation of 2%NaOH-WPL-2TESPT (as treated-biofiller), the storage modulus decreases, particularly at higher biofiller loadings (20 and 30 phr), indicating that silane coupling agents reduce stiffness, possibly by improving filler dispersion and lowering filler-filler interactions [48].

As shown in Figure 27b, all formulations exhibited a similar temperature-dependent behavior of tanδ. The peak position of tanδ, corresponding to the glass transition temperature (Tg), remained nearly unchanged across all samples, which is in agreement with the values reported in Table 10.

This trend is further supported by the data presented in Table 10, where the control sample shows a tan δ value of 0.8, reflecting strong filler–polymer interactions. The introduction of 2%NaOH-WPL-2TESPT resulted in relatively minor fluctuations in tan δ, suggesting that the addition of treated-biofiller did not significantly affect the viscoelastic behavior of the rubber composites. Furthermore, these results suggest that the energy dissipation characteristics were mainly retained, and the dynamic mechanical behavior remained comparable across all formulations containing 2%NaOH-WPL-2TESPT [6][48].

In addition, the T_g remained relatively consistent across all samples, in the range of –61.1 °C and –60.3 °C. This implies that the addition of treated-WPL did not significantly restrict the segmental motion of the polymer chains near the glass transition region. Notably, a slight increase in T_g of rubber composites containing 2%NaOH-WPL-2TESPT was possibly due to enhanced filler dispersion and interfacial interaction [6].

Table 10. T_g and tan δ_{max} values of NR/SBR composites with different 2%NaOH-WPL-2TESPT loadings.

Samples	Tan(δ_{max})	T_g (°C)
100 CB	0.8	-61.1
2%NaOH-5WPL-2TESPT	0.9	-60.4
2%NaOH-10WPL-2TESPT	~1	-60.3
2%NaOH-20WPL-2TESPT	~1	-60.4
2%NaOH-30WPL-2TESPT	~1	-61

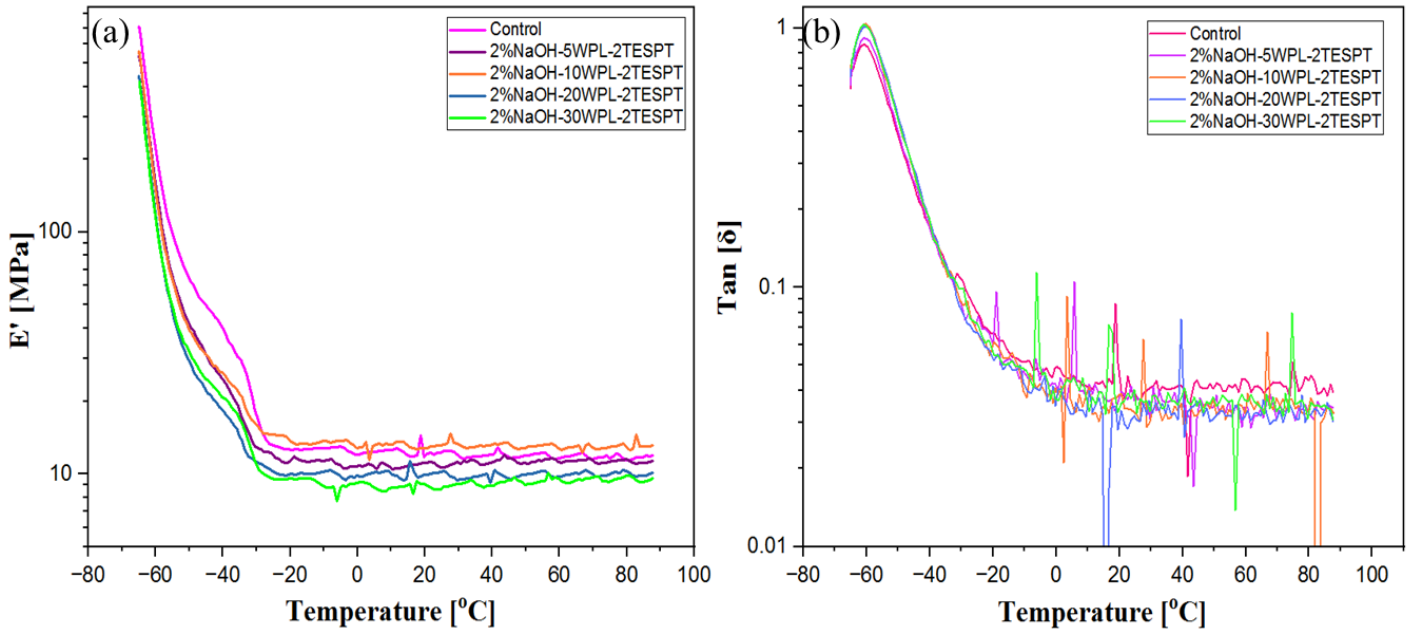

Fig. 27. DMTA results of filled-NR/SBR composites with CB/2%NaOH-WPL-2TESPT as filler, (a) E' vs. Temperature, and (b) tan δ vs. Temperature.

4.3.3. Payene effect

Another important rheological property investigated in filled-rubber composites is the Payne effect, which describes the softening of the rubber compound under induced strain. It characterizes the strength of the filler network during repetitive low-strain deformation. Quantitatively, it refers to the decrease in the elastic modulus of highly reinforced, uncured rubber as strain increases. The Payne effect can be attributed to the breakage and subsequent recovery of relatively weak physical bonds that link neighboring filler aggregates under cyclic loading. An increase in strain induces a typical reduction in the elastic modulus, and the difference between the maximum and minimum storage modulus (G′) can be used to quantify the Payne effect, denoted as ΔG′ at a particular strain. Figure 28 presents the influence of 2%NaOH-WPL-2TESPT loading on the G' and ΔG' of NR/SBR composites.

Figure 28a illustrates the variation of G' as a function of strain. At low strain levels, the control sample exhibits the highest G', confirming the strong filler-filler interactions of CB. As the strain increases, all samples show a gradual decrease in G', indicating the disruption of filler networks and a transition from a structured state to a more relaxed rubber matrix.

Figure 28b illustrates the reduction of ΔG' by increasing the treated-WPL loading. The control sample exhibits the highest ΔG' value of ~74 Pa. A higher ΔG′ value suggests stronger filler-filler

interactions, which may indicate a greater tendency for filler aggregation and agglomeration within the composite structure. In contrast, the WPL-filled rubber composites display lower ΔG' values. This reduction is attributed to decreased filler-filler interactions, as silane reacts with hydroxyl groups on Cellulose, thereby reducing hydrogen bonding. In addition, TESPT sulfur functionalities contribute to crosslinking during mixing, improved filler dispersion, and enhanced filler–rubber interactions, which result in reducing the Payne effect. This reduction typically has a positive impact on rubber composite materials, such as lower rolling resistance in tires, which improves fuel efficiency [49].

Interestingly, in the presence of 30 phr of treated WPL, ΔG' increases again, implying a potential phase transition where excessive WPL aggregation contributes to localized stress concentrations [13][3].

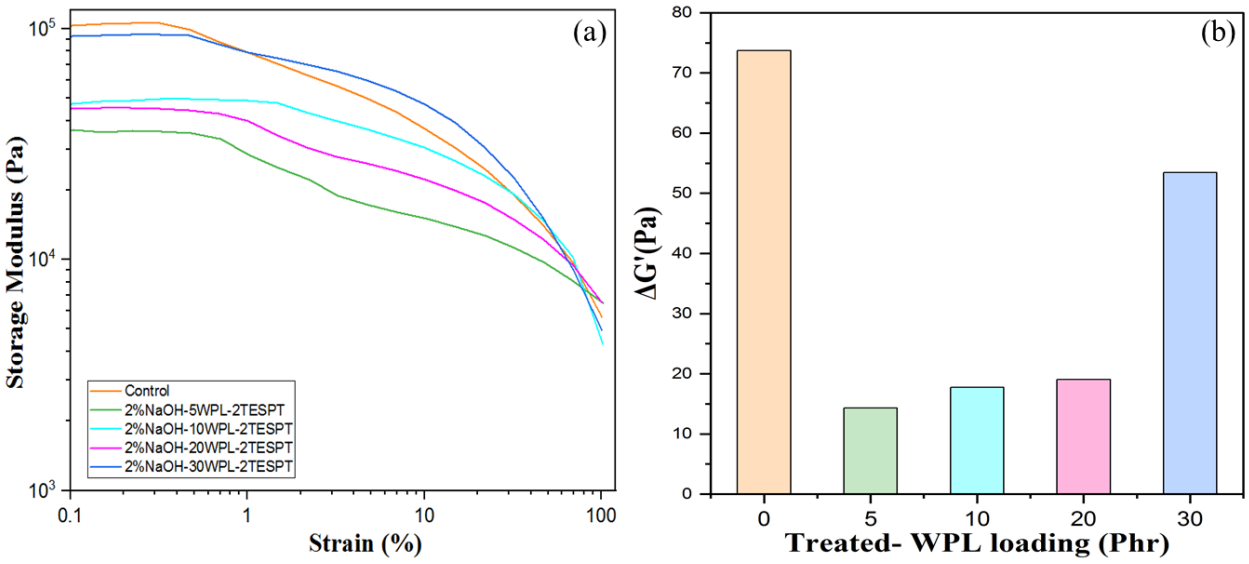

Fig. 28. Effect of 2%NaOH-WPL-2TESPT contents on (a) storage modulus as a function of strain, and b) Payne effect of filled NR/SBR composites.

4.3.4. Swelling weight ratio

The results of the swelling test are summarized in Table 12. As shown, the control sample exhibited a Q value of 1.4, indicating strong filler–matrix interactions and a dense crosslinked network. Upon partial replacement with treated-WPL, the swelling ratio initially decreased to 1.3 at 5 phr, which may be attributed to enhanced crosslink density and improved interfacial bonding that restricts solvent diffusion [35]. However, at higher biofiller loadings (10–30 phr), the Q values showed slight fluctuations within a narrow range (1.3–1.4), suggesting that further addition of

WPL does not significantly impact the solvent uptake behavior beyond a certain filler content. This may be attributed to a balance between filler aggregation and interfacial bonding, which stabilizes the network structure.

Table 11. Swelling weight ratio (Q) of NR/SBR composites containing different loadings of 2%NaOH-WPL-2TESPT biofiller.

Samples	Q
100 CB	1.4
2%NaOH-5WPL-2TESPT	1.3
2%NaOH-10WPL-2TESPT	1.4
2%NaOH-20WPL-2TESPT	1.3
2%NaOH-30WPL-2TESPT	1.4

Conclusion and Future Perspective

This thesis explored the development of sustainable NR/SBR rubber composites reinforced with WPL GS, a natural biofiller derived from winemaking by-products. To enhance the compatibility between the hydrophilic filler and hydrophobic rubber matrix, a dual surface modification strategy was adopted: alkali treatment (2 wt% NaOH) followed by silanization using TESPT at different concentrations.

The alkali treatment of WPL was carried out at various times, and the obtained samples were analyzed using different methods. SEM images showed that the alkali treatment of biofiller for 2 hours resulted in an exposed fiber structure and rougher surface morphology. FTIR spectra demonstrated reduced hemicellulose and lignin content, while TGA confirmed improved thermal stability with a higher onset degradation temperature and lower residual mass. As a result, 2%NaOH-WPL-2h was selected as the optimal alkali-treated material.

The subsequent silanization with TESPT at concentrations of 2 wt%, 5 wt%, and 10 wt% revealed that the treated samples with 2 wt% TESPT provided the most uniform and effective surface modification. ATR FTIR analysis of the combined alkali-silane-treated WPL confirmed successful chemical grafting, with new peaks appearing at 2972 cm^{-1} and 2920 cm^{-1} (C–H stretching from TESPT) and attenuation of O–H stretching vibrations around 3326 cm^{-1}, suggesting reduced hydrophilicity. Although some silane peaks overlapped with cellulose bands, additional SEM-EDX analysis confirmed the presence and uniform distribution of silicon and sulfur in the treated samples. TGA analysis confirmed that the incorporation of TESPT improved

the thermal stability of the treated samples. The 2 wt% TESPT-treated WPL exhibited the highest Tmax (336 °C) and char residue at 700 °C (33.9 wt%), indicating a more thermally stable silane-modified structure due to better dispersion and interaction with the fiber surface. Also, the grafted TESPT content reached 0.76 mmol/g for the 2 wt% TESPT sample, which proved optimal in terms of dispersion and thermal behavior.

Rubber composites were formulated with varying amounts of 2% NaOH-WPL-2TESPT (5, 10, 20, and 30 phr) as biofiller and CB, to evaluate the effect of filler loading. Mechanical testing indicated that the composite containing 10 phr treated-WPL achieved tensile strength comparable to the control sample (11 MPa), while improving modulus and preserving elongation. At higher biofiller loadings, tensile strength declined slightly due to filler agglomeration, whereas overall mechanical integrity remained acceptable.

DMTA analysis indicated that tan δ remained nearly unchanged across all samples, confirming that damping behavior and energy dissipation were not significantly affected by biofiller substitution. The glass transition temperature showed minimal variation, indicating that polymer chain mobility remained intact. Moreover, swelling behavior was consistent across all filler loadings, confirming good crosslinking and chemical bonding. The Payne effect decreased at lower treated WPL loadings, suggesting weaker filler-filler interactions and better filler dispersion compared to control sample.

In summary, this study demonstrated that up to 30 phr of treated WPL (combined alkali-silene treatment) can be used as a partial replacement for carbon black in NR/SBR composites without compromising mechanical, thermal, or dynamic properties. The dual alkali-silane treatment significantly enhances biofiller performance, offering a renewable and eco-friendly solution for rubber composite reinforcement. These findings support the industrial viability of lignocellulosic fillers in sustainable tire technologies and contribute to reducing dependence on petroleum-based materials.

Based on the encouraging findings of this study, various future research avenues may be explored to enhance the advancement of sustainable rubber composites with lignocellulosic biofillers:

1. Advanced Surface Characterization:

Techniques such as FTIR mapping, XPS, or solid-state NMR could be employed to better understand the interfacial interactions between treated biofillers and the rubber matrix, including silane grafting efficiency and network formation.

2. Processability and Industrial Feasibility:

Pilot-scale processing of optimized composites is essential to assess scalability, dispersion quality, and reproducibility using standard mixing and vulcanization equipment in industrial environments.

3. Environmental and Long-Term Performance Assessment:

Future studies should evaluate aging, weathering, and mechanical fatigue under real conditions, and conduct life cycle assessment (LCA) to quantify the environmental benefits of treated biofillers over traditional carbon black fillers.

These future directions can facilitate the broader implementation of sustainable rubber technologies and significantly diminish the environmental impact of elastomer-based industries.

References

[1] M. Dadkhah and M. Messori, “A comprehensive overview of conventional and bio-based fillers for rubber formulations sustainability,” Sep. 01, 2024, *Elsevier Ltd*. doi: 10.1016/j.mtsust.2024.100886.

[2] Y. Hou and W. Wu, “Derived from corn straw cellulose: modified used tire rubber powder composites,” *Cellulose*, vol. 29, no. 7, pp. 3935–3945, May 2022, doi: 10.1007/s10570-022-04549-y.

[3] J. Miedzianowska, M. Masłowski, and K. Strzelec, “Improving performance of natural rubber composites by the application of functional biofiller - horsetail modified with silane coupling agents,” Feb. 21, 2023. doi: 10.21203/rs.3.rs-2596406/v1.

[4] M. Dominic, R. Joseph, P. M. Sabura Begum, B. P. Kanoth, J. Chandra, and S. Thomas, “Green tire technology: Effect of rice husk derived nanocellulose (RHNC) in replacing carbon black (CB) in natural rubber (NR) compounding,” *Carbohydrate Polymers*, vol. 230, Feb. 2020, doi: 10.1016/j.carbpol.2019.115620.

[5] H. Kazemi, F. Mighri, and D. Rodrigue, “A Review of Rubber Biocomposites Reinforced with Lignocellulosic Fillers,” Jul. 01, 2022, *MDPI*. doi: 10.3390/jcs6070183.

[6] T. H. Mokhothu, A. Mtibe, T. C. Mokhena, and M. J. Mochane, “Influence of silane modification on the properties of natural fibers and its effect on biocomposites,” in *Surface Treatment Methods of Natural Fibres and their Effects on Biocomposites*, Elsevier, 2022, pp. 67–93. doi: 10.1016/B978-0-12-821863-1.00004-1.

[7] M. Masłowski, J. Miedzianowska, and K. Strzelec, “Natural Rubber Composites Filled with Cereals Straw Modified with Acetic and Maleic Anhydride: Preparation and Properties,” *Journal of Polymers and the Environment*, vol. 26, no. 10, pp. 4141–4157, Oct. 2018, doi: 10.1007/s10924-018-1285-5.

[8] Y. Liu, J. Xie, N. Wu, Y. Ma, C. Menon, and J. Tong, “Characterization of natural cellulose fiber from corn stalk waste subjected to different surface treatments,” *Cellulose*, vol. 26, no. 8, pp. 4707–4719, May 2019, doi: 10.1007/s10570-019-02429-6.

[9] M. J. John and S. Thomas, “Biofibres and biocomposites,” Feb. 08, 2008. doi: 10.1016/j.carbpol.2007.05.040.

[10] M. M. Kabir, H. Wang, K. T. Lau, and F. Cardona, “Chemical treatments on plant-based natural fibre reinforced polymer composites: An overview,” *Composites Part B: Engineering*, vol. 43, no. 7, pp. 2883–2892, Oct. 2012, doi: 10.1016/j.compositesb.2012.04.053.

[11] B. Teshome Wagaye *et al.*, “Textile & Leather Review A Review of Cellulosic Fibre Surface Modification Techniques-The Case of Ramie A Review of Cellulosic Fibre Surface Modification Techniques-The Case of Ramie,” vol. 7, pp. 1061–1095, 2024, doi: 10.31881/TLR.

[12] A. K. Bledzki and J. Gassan, “Composites reinforced with cellulose based fibres,” 1999.

[13] W. Kaewsakul, K. Sahakaro, W. K. Dierkes, and J. W. M. Noordermeer, “Mechanistic aspects of silane coupling agents with different functionalities on reinforcement of silica-filled natural rubber

compounds," *Polymer Engineering and Science*, vol. 55, no. 4, pp. 836–842, Apr. 2015, doi: 10.1002/pen.23949.

[14] K. Roy, S. C. Debnath, L. Tzounis, A. Pongwisuthiruchte, and P. Potiyaraj, "Effect of various surface treatments on the performance of jute fibers filled natural rubber (NR) composites," *Polymers*, vol. 12, no. 2, Feb. 2020, doi: 10.3390/polym12020369.

[15] N. A. M. Nor and N. Othman, "Effect of Filler Loading on Curing Characteristic and Tensile Properties of Palygorskite Natural Rubber Nanocomposites," *Procedia Chemistry*, vol. 19, pp. 351–358, 2016, doi: 10.1016/j.proche.2016.03.023.

[16] J. Miedzianowska, M. Masłowski, P. Rybinski, and K. Strzelec, "Properties of chemically modified (selected silanes) lignocellulosic filler and its application in natural rubber biocomposites," *Materials*, vol. 13, no. 18, Sep. 2020, doi: 10.3390/ma13184163.

[17] J. Fröhlich, W. Niedermeier, and H. D. Luginsland, "The effect of filler-filler and filler-elastomer interaction on rubber reinforcement," *Composites Part A: Applied Science and Manufacturing*, vol. 36, no. 4, pp. 449–460, 2005, doi: 10.1016/j.compositesa.2004.10.004.

[18] Z. Gu *et al.*, "Preparation and properties of styrene butadiene rubber/natural rubber/organo-bentonite nanocomposites prepared from latex dispersions," *Applied Clay Science*, vol. 46, no. 3, pp. 241–244, 2009, doi: 10.1016/j.clay.2009.08.010.

[19] P. Saha, S. Chowdhury, D. Roy, B. Adhikari, J. K. Kim, and S. Thomas, "A brief review on the chemical modifications of lignocellulosic fibers for durable engineering composites," *Polymer Bulletin*, vol. 73, no. 2, pp. 587–620, 2016, doi: 10.1007/s00289-015-1489-y.

[20] P. S. Rai, S. Unnikrishnan, and A. Chandrashekar, "Influence of alkali treatment on physiochemical and morphological properties of palmyra fibers," *Industrial Crops and Products*, vol. 224, no. July 2024, p. 120298, 2025, doi: 10.1016/j.indcrop.2024.120298.

[21] M. S. S. Godara, "Effect of chemical modification of fiber surface on natural fiber composites: A review," *Materials Today: Proceedings*, vol. 18, pp. 3428–3434, 2019, doi: 10.1016/j.matpr.2019.07.270.

[22] W. Gieparda, M. Przybylak, S. Rojewski, and B. Doczekalska, "Polysiloxanes and Silanes with Various Functional Groups—New Compounds for Flax Fibers' Modification," *Materials*, vol. 16, no. 10, May 2023, doi: 10.3390/ma16103839.

[23] A. Karthik, M. Bhuvaneshwaran, M. S. Senthil Kumar, S. Palanisamy, M. Palaniappan, and N. Ayrilmis, "A Review on Surface Modification of Plant Fibers for Enhancing Properties of Biocomposites," Jun. 04, 2024, *John Wiley and Sons Inc*. doi: 10.1002/slct.202400650.

[24] Y. Zhou, M. Fan, and L. Chen, "Interface and bonding mechanisms of plant fibre composites: An overview," *Composites Part B: Engineering*, vol. 101, pp. 31–45, 2016, doi: 10.1016/j.compositesb.2016.06.055.

[25] N. Jardon-Maximino, M. Dehonor Gómez, R. Villa Moreno, M. D. Baeza-Alvarado, and L. E. Lugo Uribe, "Optimization of the Alkali-Silane Treatment of Agave lechuguilla Fibers (Ixtle) for Potential

Reinforcement in Polymeric Composites," *Fibers*, vol. 11, no. 10, Oct. 2023, doi: 10.3390/fib11100086.

[26] D. Bachtiar, S. M. Sapuan, and M. M. Hamdan, "The effect of alkaline treatment on tensile properties of sugar palm fibre reinforced epoxy composites," *Materials and Design*, vol. 29, no. 7, pp. 1285–1290, 2008, doi: 10.1016/j.matdes.2007.09.006.

[27] P. Saha, S. Manna, S. R. Chowdhury, R. Sen, D. Roy, and B. Adhikari, "Enhancement of tensile strength of lignocellulosic jute fibers by alkali-steam treatment," *Bioresource Technology*, vol. 101, no. 9, pp. 3182–3187, May 2010, doi: 10.1016/j.biortech.2009.12.010.

[28] E. Widodo, Pratikto, Sugiarto, and T. D. Widodo, "Comprehensive investigation of raw and NaOH alkalized sansevieria fiber for enhancing composite reinforcement," *Case Studies in Chemical and Environmental Engineering*, vol. 9, Jun. 2024, doi: 10.1016/j.cscee.2023.100546.

[29] R. Z. Raia, S. Iwakiri, R. Trianoski, A. S. de Andrade, and E. L. Kowalski, "Effects of alkali treatment on modification of the pinus fibers," *Revista Materia*, vol. 26, no. 1, 2021, doi: 10.1590/s1517-707620210001.1236.

[30] J. I. ; N. D. E. ; M. J. R. ; R. N. W. M. ; S. J. H. J. ; J. D. C. Goldstein, *Scanning Electron Microscopy and X-ray Microanalysis*, 4th ed. Springer, 2018.

[31] B. Stuart, *Infrared Spectroscopy: Fundamentals and Applications*, 1st ed. John Wiley & Sons, 2004.

[32] "1-IntroductiontoThermalAnalysisTechniquesandApplications".

[33] K. P. Menard and N. R. Menard, "Dynamic Mechanical Analysis; Third Edition."

[34] "Materials Science and Engineering An Introduction by William D. Callister, Jr., David G. Rethwish (z-lib.org)".

[35] H. Kazemi, F. Mighri, K. W. Park, S. Frikha, and D. Rodrigue, "Natural rubber biocomposites reinforced with cellulose nanocrystals/lignin hybrid fillers," *Polymer Composites*, vol. 43, no. 8, pp. 5442–5453, Aug. 2022, doi: 10.1002/pc.26846.

[36] O. Somseemee, P. Sae-Oui, and C. Siriwong, "Reinforcement of surface-modified cellulose nanofibrils extracted from Napier grass stem in natural rubber composites," *Industrial Crops and Products*, vol. 171, Nov. 2021, doi: 10.1016/j.indcrop.2021.113881.

[37] B. W. Chieng, S. H. Lee, N. A. Ibrahim, Y. Y. Then, and Y. Y. Loo, "Isolation and characterization of cellulose nanocrystals from oil palm mesocarp fiber," *Polymers*, vol. 9, no. 8, Aug. 2017, doi: 10.3390/polym9080355.

[38] T. Cionita *et al.*, "The Influence of Filler Loading and Alkaline Treatment on the Mechanical Properties of Palm Kernel Cake Filler Reinforced Epoxy Composites," *Polymers*, vol. 14, no. 15, Aug. 2022, doi: 10.3390/polym14153063.

[39] H. Kargarzadeh, I. Ahmad, I. Abdullah, A. Dufresne, S. Y. Zainudin, and R. M. Sheltami, "Effects of hydrolysis conditions on the morphology, crystallinity, and thermal stability of cellulose nanocrystals extracted from kenaf bast fibers," *Cellulose*, vol. 19, no. 3, pp. 855–866, Jun. 2012, doi: 10.1007/s10570-012-9684-6.

[40] D. Ray, B. K. Sarkar, R. K. Basak, and A. K. Rana, “Study of the thermal behavior of alkali-treated jute fibers,” *J. Appl. Polym. Sci.*, vol. 85, no. 12, pp. 2594–2599, Sep. 2002, doi: 10.1002/app.10934.

[41] S. A. Kavitha, K. P. Retnam, K. P. Arunachalam, M. Abbas, C. B. Ávila, and S. Avudaiappan, “Effect of Alkali and Permanganate Treatments on Terminalia catappa Leaf Fibers: Efficient Reinforcements to Be Used in Eco-Friendly Composites,” *ACS Omega*, vol. 10, no. 15, pp. 14566–14580, 2025, doi: 10.1021/acsomega.4c02715.

[42] N. Lopattananon, D. Jitkalong, and M. Seadan, “Hybridized reinforcement of natural rubber with silane-modified short cellulose fibers and silica,” *Journal of Applied Polymer Science*, vol. 120, no. 6, pp. 3242–3254, Jun. 2011, doi: 10.1002/app.33374.

[43] A. K. Balan, S. Mottakkunnu Parambil, S. Vakyath, J. Thulissery Velayudhan, S. Naduparambath, and P. Etathil, “Coconut shell powder reinforced thermoplastic polyurethane/natural rubber blend-composites: effect of silane coupling agents on the mechanical and thermal properties of the composites,” *Journal of Materials Science*, vol. 52, no. 11, pp. 6712–6725, Jun. 2017, doi: 10.1007/s10853-017-0907-y.

[44] A. M. P B Samarasekara, K. D. H N Kahavita, D. Amarasinghe, and L. Karunanayake, “Fabrication and Characterization of Nanofibrillated Cellulose (NFC) Reinforced Polymer Composite; Fabrication and Characterization of Nanofibrillated Cellulose (NFC) Reinforced Polymer Composite,” 2018.

[45] P. Skalková, Z. Mičicová, I. Papučová, J. Pagáčová, I. Labaj, and B. Pecušová, “OPTIMAL PROPERTIES OF SURFACE MODIFIED CELLULOSE AS FILLER IN POLYMER COMPOSITES,” 2024.

[46] E. Robles, L. Csóka, and J. Labidi, “Effect of reaction conditions on the surface modification of cellulose nanofibrils with aminopropyl triethoxysilane,” *Coatings*, vol. 8, no. 4, Apr. 2018, doi: 10.3390/coatings8040139.

[47] U. Moonart and S. Utara, “Effect of surface treatments and filler loading on the properties of hemp fiber/natural rubber composites,” *Cellulose*, vol. 26, no. 12, pp. 7271–7295, Aug. 2019, doi: 10.1007/s10570-019-02611-w.

[48] P. Jantachum, B. Khumpaitool, and S. Utara, “Effect of silane coupling agent and cellulose nanocrystals loading on the properties of acrylonitrile butadiene rubber/natural rubber nanocomposites,” *Industrial Crops and Products*, vol. 195, May 2023, doi: 10.1016/j.indcrop.2023.116407.

[49] T. H. Chang, B.P.; Gupta, A.; Muthuraj, R.; Mekonnen, “Bioresourced Fillers for Rubber Composite Sustainability: Current Development and Future Opportunities,” *Green Chem.*, vol. 23, pp. 5337–5378, 2021, doi: 10.1039/D1GC01115D.